AD-A189 927 VISUALIZATION OF FLOWS IN TURBOMACHINERY(U) TECHNION - 1/1
ISRAEL INST OF TECH HAIFA I IANOVICI ET AL. DEC 87
AFOSR-85-0308

UNCLASSIFIED NL

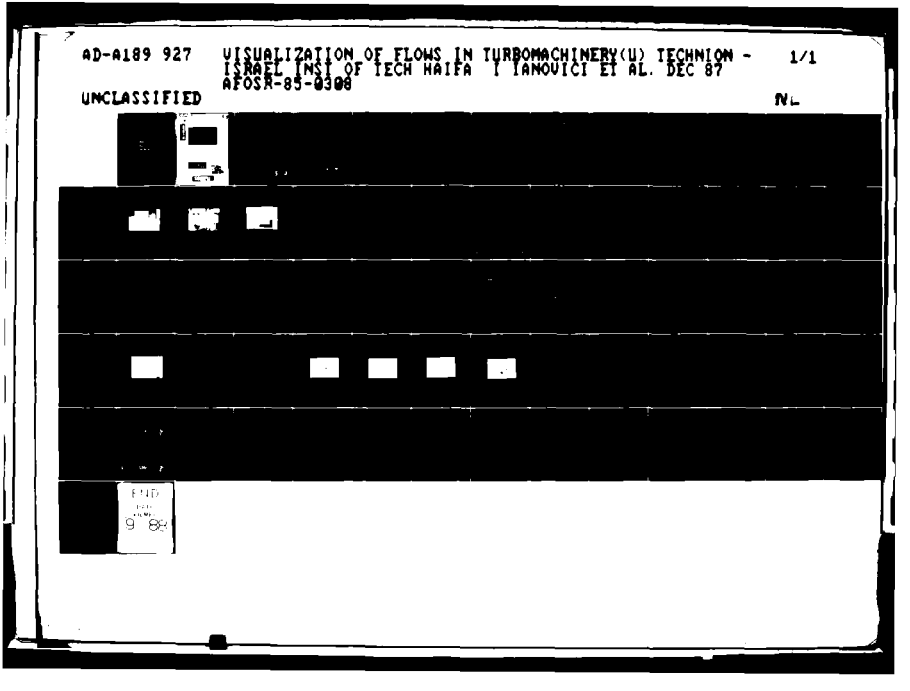

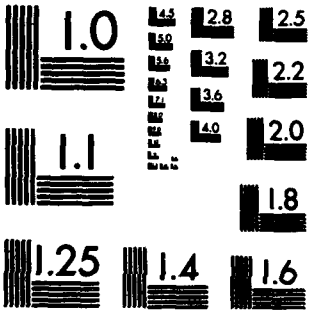
1.0
1.1
1.25
1.4
1.6
1.8
2.0
2.2
2.5
2.8
3.2
3.6
4.0
4.5
5.0

VISUALIZATION OF FLOWS

IN TURBOMACHINERY

VISUALIZATION OF FLOWS

IN TURBOMACHINERY

AFOSR-85-0308

by Ianovici I. and D. Adler

Technion - Haifa
Faculty of Mechanical Engineering

December 1987

ABSTRACT

A method of gas flow visualization based on laser induced fluorescence has been theoretically and experimentally investigated.

Liquid droplets seeded with fluorescent substance were introduced locally in an air flow. A laser light sheet is used to scan the flow field. The light emitted by the fluorescent substance is used to obtain, after filtering the image of a point on a specific streamline.

The method has been applied to the visualization of streamlines around a cylinder.

The possibility of the use of this method in the visualization of flows in turbomachines has been investigated. Some of the main features of the necessary equipment have been defined too.

KEY WORDS:

Visualization, gas flow, laser induced fluorescence.

CONTENTS

1. GENERAL

1.1 Fluid flow in turbomachinery-characteristics.

The specific characteristics of the fluid flow in the turbomachines are heavily conditioning the experimental methods to be used for their investigation.

Under normal conditions the fluids flowing through the turbomachines are mixtures of gases (O_2, N_2; CO_2; a.s.o.). The flows are viscous and turbulent. Sometimes chemical reactions also take place (i.e. burning) but our investigation does not cover these flows.

The solid boundaries are, generally, asymetric, with numerous changes in curvature radius. Under normal conditions some of these boundaries are in rotational movement, mostly at high speeds. They are usually of metal (alloys).

Technological and functional conditions (i.e. tip clearances) lead to some supplementary flows (or perturbating factors).

High pressures and temperatures are frequently encountered (with non-uniform distributions).

All the abovementioned factors contribute to the appearance of highly complicated flow paterns even in simpler cases (subsonic, low temperatures, no chemical reactions, no rotating boundaries).

1.2 Visualization method

1.2.1 Utility

The visulization methods allow direct perception either by eye or similar apparatus (photgraphic, film, camera) of one or several properties of the fluid flow. Because of the complexity of the phenomena, the visualization of the flows in turbomachinery is preceeding, almost in all cases, any modern research whether theoretical (mathematical modelling) or experimental (measurements of flow characteristics). Ref. [1] describes a visualization method (coloured smoke) used to obtain a first description of horseshoe and passage vortices in turbine-blade passage. The authors reached the conclusion that these vortices cannot exist independently. Ref. [2] is one of the few efforts to observe directly the Gortler and Karman vortices on the pressure side and trailing edge of a static blade cascade. The influence of the geometry of the blades has been investigated. An extensive study of the tip region of a rotating blade row is described in ref. [3]. The effect of the tip clearance on the end-wall boundary layer is investigated. Several important conclusions are presented of which we quote: "The photographs exhibit no direct evidence of blade boundary layer fluid beying centrifuged into the end-wall layer". A very interesting study combining visualization with pressure measurements on the blade (in a water analogy rig) is presented in ref. [4]. The study allowed the authors to reach conclusions on the practical design of the blade tip: "...Such efficiency improvement is most likely to be obtained on rather thick blades, indicating that mini-shrouds (winglets) may be desirable, especially for thin

blades". The visualization methods can be extended to quantitative investigations too, using modern image processing techniques. Ref. [5] shows aerosol sprays being automatically mapped (contours built by computer). Ref. [6] presents the use of a visualization technique to build density maps in a transonic compressor rotor. Here too the primary photographs (images) are corrected with the aid of a computer and new maps are drawn. Ref. [7] makes an extensive analysis of the severe requirements imposed on any visualizing method to be applied for turbomachinery flows. Still: "Quantification and validation can then follow via the hard data provided by anemometry guided by what has already been seen". A visualization method must help to locate favourably other instruments (i.e. thermocouples; pressure transducers; a.s.o.) and reveal regions of separation, vortexes a.s.o.

1.2.2 Main features.

1.2.2.1 The information carrier is light and the path between the light source and the collector is made up of linear segments (no optic fibers used.).

1.2.2.2 A flow property is translated into an image.

1.2.2.3 This translation is usually realized by an intermediate element called tracer. It has to be different from the fluid (optical properties) but has to behave similarly from aerodynamic point of vue (velocity, direction of movement a.s.o.).

1.2.2.4 The visual methods have to (and do, generally) produce low level energy perturbations in the studied flows. Care has to be taken not to produce important local changes either on the fluid or the tracer particles when high energy exciting beams are used (or focused).

2. VISUALIZATION METHOD SELECTION.

The key element in the selection of a visualization method is the tracer. According to the specific behaviour of each tracer type under illumination (radiation) the methods can be grouped in reflection or absorption/emission type. Illumination (radiation) with rays out of the visible range (uv, x, gamma, a.s.o.) has not been investigated in the present work.

2.1 Methods based on light reflection.

These methods use a multimolecular tracer which reflects most of the incidient light. Such tracers might be either liquid or solid. Ref. [8] describe a smoke generator. The smoke is composed of micron size solid ash particles which reflect the incident light beam. Ref. [9] describes a tracer of liquid (oil drops, water drops). Both types of tracers have been used in studies of flows in wind tunnels or turbomachines. Ref. [10] and [11] describe the use of smoke tracers to the study of three dimensional flows around bodies in wind tunnels (ONERA - France). Ref. [3] describes the use of smoke in a moving rotor.

The main deficiency of these methods consists in the high level of "noise" in the collected image: the incident light and the reflected one are of the same type (wavelength) and the solid boundaries (metallic) reflect light too. Therefore contrast between tracer image and the rest of the environment is poor. Specific methods have been devised for boundary layer flows. Ref. [12] presents traces of ink on paper, in a cascade of turbine blades mounted in a wind tunnel. "The traces represent an approximation to limiting streamlines". A similar type of visualization using ammonia and Ozalid paper has been used in a rotor, in movement, ref. [13]. A stroke light was used to achieve clear traces on the paper.

Some important practical conclusions have to be drawn:

a. there are no special requirements for the investigated fluid and flow (natural air, standard rotor and casings, open circuit wind tunnel, a.s.o.).

b. the tracers are available in a wide range (solids, liquids) and considerable experience has been accumulated in the production and distribution of these tracers in the flows.

c. the light source and the light collecting device are very usual ones (commercial lamps, photographic apparatuses).

d. there is no "universal" method for both the bulk and the boundary layers because of the high level "noise" associated with this type of visualization.

2.2 Methods based on light emission.

These methods are based on the photo-luminescence phenomenon which is luminescence (light emission) under light stimulation: "Fluorescence means a luminescence stimulated by radiation, not continuing more than 10^{-8} sec. after the stimulating radiation is cut off" [14]. Under the stimulating radiation atoms raise to a higher energy level, but return soon to a lower state by

emitting a new radiation. The wavelength of this new radiation might be higher than the incident one (according to Stokes' law). In some cases this wavelength might be smaller and it is called "anti Stokes radiation". For fluids, the quenching phenomenon has to be kept in mind: The stimulated molecules (atoms) collide with other molecules and energy is transferred to them. The number of collisions per second per atom is specific for each fluid of course, to the pressure and temperature conditons, [14].

Despite the complicated problems which arrise when using these methods a great advantage has to be born in mind: these tracers allow, with adequate filtering, to separate the emitted light form the incident one (if UV light is used for stimulation too). The emitted light can be collected at any angle because it is randomly polarised and the intensity is independent of the direction [47].

Since the stimualtion is at molecular/atomic level, the tracer substances have to be dispersed down to this level, i.e. they have to be either in gaseous state or in liquid solutions with highly transparent liquids or solids. Ref. [15] presents an experimental study in wind tunnels: "extremely thin fluoresent nylon" filaments (0.02 mm diameter) are attached to the studied surfaces and illuminated with ultraviolet radiation. " . . . a barrier filter (is placed) over the camera lens, which passes the visible fluorescence and blocks the reflected ultraviolet".

A special technique was used in ref. [16] in order to investigate the flow around a wing in motion. "The models were towed in a water channel and several thin, . . . sheets of fluorescent dye were excited with a sheet of laser light to visualize the complex, unsteady separated flow around each wing". Fluorescein, Rhodamine B and Rhodamine 6G were used (good solubility in water). Ref. [17] investigates the supersonic cold flow mixing between slit nozzles. The visualization technique uses iodine vapor as tracer. It is excited by a green argon ion laser beam. "If a narrow-band optical filter is used to block the green pumping (exciting) beam, a planar cross section of the fluorescing steam can be observed or rercorded. . .". Although not presenting a visualization method proper, ref. [18] describes the use of a gas tracer (biacetyl) "especially suitable for seeding gas flows". Since quenching in oxygen is very important the experiments had to be conducted in nitrogen and. . . the system was thoroughly leak checked to exclude oxygen.".

The substances having luminescent properties have a specific wavelength of maximum absorption of the stimulating light and a specific wave length of emission. Therefore a high energy beam of prescribed wavelength can be obtained only by using lasers as sources. Ref. [19] presents an extensive revue of measurements in gas flows using laser-induced fluorescence. An important conclusion is drawn by the authors: "Condensation is a significant problem with most of the substances that can be used with the presently (1983) available laser wavelengths. . .". "Of most interest to gas-dynamic applications is the column* for future lasers having wavelengths of 230nm or less with which argon could be excited to 106.7nm. . .".

Several researchers used the laser-induced fluorescence technique in velocity

measurements. The fluorescent tracers produce Doppler shift of the emitted radiation frequency due to their movement. [20], [21]. The main advantage is that fluorescence is isotropic and allows to work with the receiving optics in whatever direction and with large aperture (collecting angles). Allthough the signal is lower than that of standard laser-Doppler ". . . filtering can be very efficient in reducing the high back-ground noise problem, common to some LDA systems, particularly in boundary layer applications. . .".

A special group of light emission methods is based on electrical discharge stimulation. A ionized column of particles is created between two electrodes by an electric discharge. A series of succeeding sparks will folllow the ionized column and illuminate it. The gas flow will displace the column. If the parameters of the sparks are known (durations, disturbances a.s.o.) valuable information can be obtained from the photographs. [22]. This method has been applied both to stationary set-ups and for moving impellers [23]. This mehtod requires severe insulation and the material of the impeller has to be non-metalic. If local investigation of the flow is to be conducted it has to be born in mind that any type of electrodes do disturb the flow.

2.3. Selected method.

2.3.1. Purpose

The purpose of the method selected in the present work is limited to the visualization of the streamlines in a gas flow, despite the placement of the line (bulk or boundary layer). The flow is cold and no chemical reactions take place.

The first stage of the study has to prove the feasibility of the method and its application to a stationary set-up.

2.3.2. Selection.

The methods based on light reflection have been discarded from the beginning because the high level of noise produced by walls and the incident light (all of the same wavelengths). The methods based on electric discharges were also discarded because of the significant disturbances introduced in the flow by the electrodes.

The main target of the work was to determine the fundamental characteristics of a light emission based method and check its feasibility. Table 2.3.2-1. presents the requirements and the possibilities in the laboratory of the Technion - Haifa.

Table 2.3.2.-1.

Tracer type*	Carrier type	Investi-gated fluid	Necessary//Available Equipment					
			Monochrom. light source	Seeder	Wind tunnel		Collecting optics	
					closed	open	amplifier**	recording
Gas	-	Not air	Yes/Yes	Yes/Not	Y/N	N/N	N/N	Y/Y
Atom	-	Not air	Yes/Yes	Yes/Not	Y/N	N/N	N/N	Y/Y
Solid	-	Normal air	Yes/Yes	Yes/Not	N/N	N/N	Y/N	Y/Y
Solid	Liquid	Normal air	Yes/Yes	Yes/Yes	N/N	N/Y	Y/N	Y/Y

Note:

* The name "gas" applies to molecules of substances in gaseous state.

** Amplification is referred to light intensity.

Several comments have to be made from the beginning:

- At this stage we did not take into account the market prices of the substances or the equipment necessary and not available in the laboratory.
- The equipment necessary to get the tracer substances from its marketing form to the used one (in table) has not been taken into account.
- Since our interpretation of visualizing is of the classical type no electronic device (including computer) has been taken into account in the collecting-recording section.
- The collecting-amplification device is considered necessary (a priori) for the cases using normal air on the base of a higher quenching and unknown impurities.

Both closed and open type tunnels need filtering either in order to keep the investigated fluid clean or to avoid damaging the environment.

All the alternatives require a seeding apparatus. It has to introduce the tracer in a required quantity in the investigated region. For the case of a liquid carrier some experience was available from the laser-Doppler anemometry techniques.

The case of a solid tracer with a solid carrier (nylon with fluorescent dye for example) has not been investigated because no such carrier has been found on the market.

Taking into account all the pro's and con's the solid tracer in a liquid type carrier in conjunction with an open type wind tunnel has been selected as the mainframe of the experiment.

3. TEST RIG

The main elements of the test rig were already available in the laboratory and our efforts concentrated on adapting them to our experiments.

3.1 Wind tunnel

An open type wind tunnel made of perspex (1) was linked to a centrifugal fan (2). The fan is entrained by variable speed electrical motor (3). The wind tunnel has a rectangular section. A Pitot tube (4) was installed to estimate the free velocity. A schematic view of this arrangement is shown in fig. 3.1. - 1.

A special arrangement was devised for the test section. A cylinder was placed in the wind tunnel axis for the first stage of the experiments. The seeder had to be introduced in the flowing air at various positions around the cylinder in order to achieve the mapping (i.e. tracing) of various stream lines. The liquid carrier droplets are to be introduced into the flowing air through a hypodermic needle with 0.55mm diameter. Fig. 3.1.-2. to 4 show the arrangement as used in the experiments. Appendix 1 contains the detailed drawings of the test section. An eccentric discs system has been used for the correct* placement of the needle tip and axis in the test section (relative to the cylinder) - fig. 3.1. - 5. (and picture shown in fig. 3.1. - 4.). In order to place the tip at a given x-y position the angles $\alpha - \beta$ have been calculated with eq. 3.1. - 1,2. In order to achieve an isokinetic introduction of the droplets the direction of the velocity vector has to be also given by the hypodermic needle. The support of the needle (fig. 3.1. - 3.) allows for any angle to be obtained. Both the discs were marked for the reading of the angles. The positioning is manually achieved.

$$\beta = \arcsin\left[\frac{R_2}{R}\cdot\sqrt{1-\left(\frac{R^2+R_1^2-R_2^2}{2R_1R}\right)^2}\right] \qquad \text{eq. 3.1. - 1}$$

$$\alpha = \arctg\left(\frac{y}{x}\right) + \arcsin\left[\sqrt{1-\left(\frac{R^2+R_1^2-R_2^2}{2R_1R}\right)^2}\right] \qquad \text{eq. 3.1. - 2.}$$

Glass windows were provided on two perpendicular walls of the tunnel.

Several characteristics of the test rig are listed in table 3.1. - 1.

---

* Note

Since the flow is two dimensional in this case the needle needs not to be positioned in the third

dimension and its axis is fixed at 90° to the cylinder axis (i.e. parallel to the tunnel floor).
A summary analysis of the precision of the needle tip positioning mechanism is presented in appendix 2.

Table 3.1. - 1.

Parameter	Units	Value
Inlet section height - H	m	0.049
Inlet section width - W	m	0.200
Inlet section area - A	m^2	0.0098
Inlet section hydr. radius RH	m	0.0197
Test section distance-L	m	0.220
Maximum average velocity in free section *	m/s	~ 50
Maximum average velocity in minimum flow section	m/s	~ 75
Reynolds number in test section	-	1500000

*Note
This value has been determined using a Pitot tube placed in the mid section of the wind tunnel.

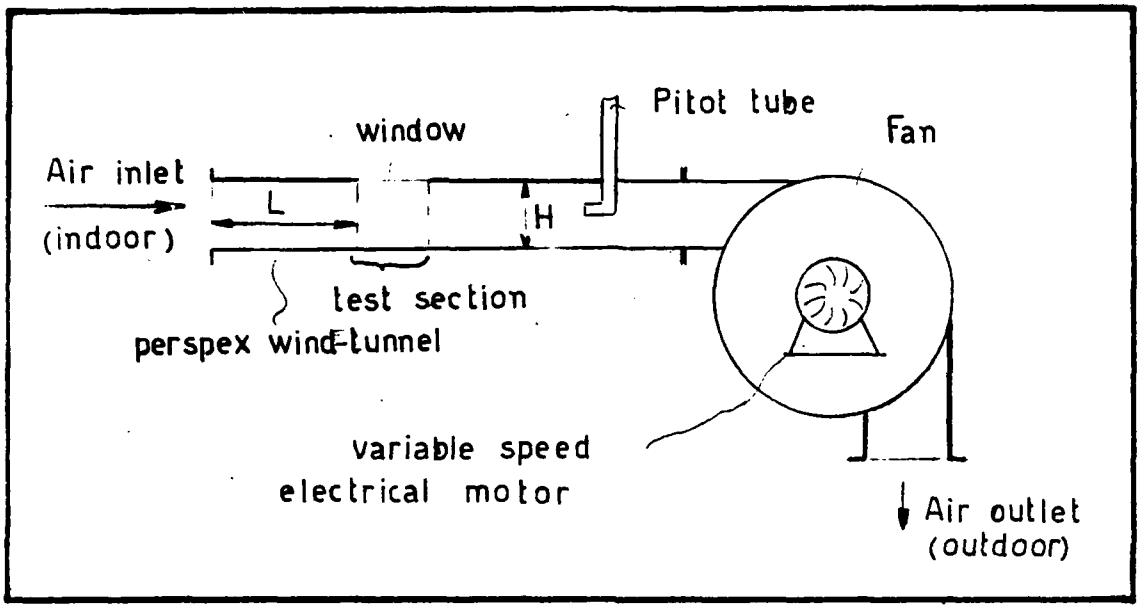

fig. 3.1-1: general arrangement of wind tunnel.

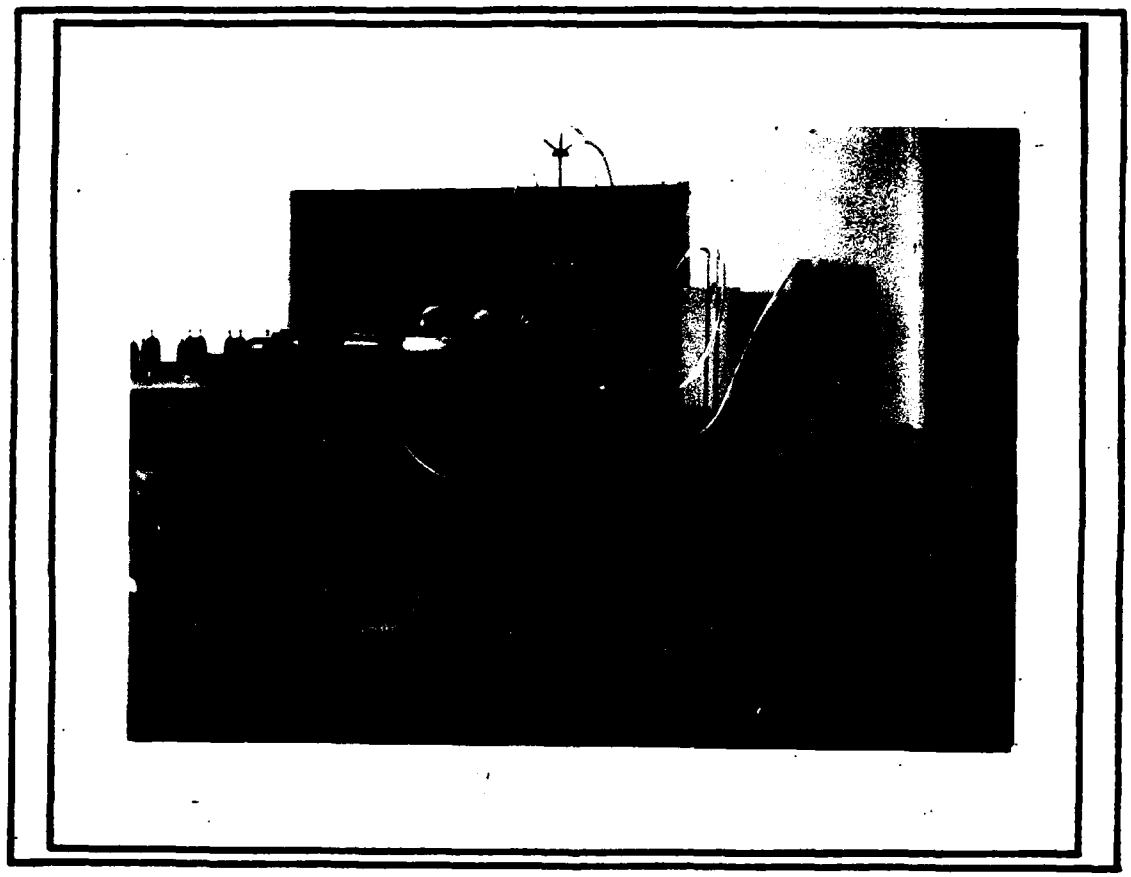

fig. 3.1-2: test rig — general arrangement.

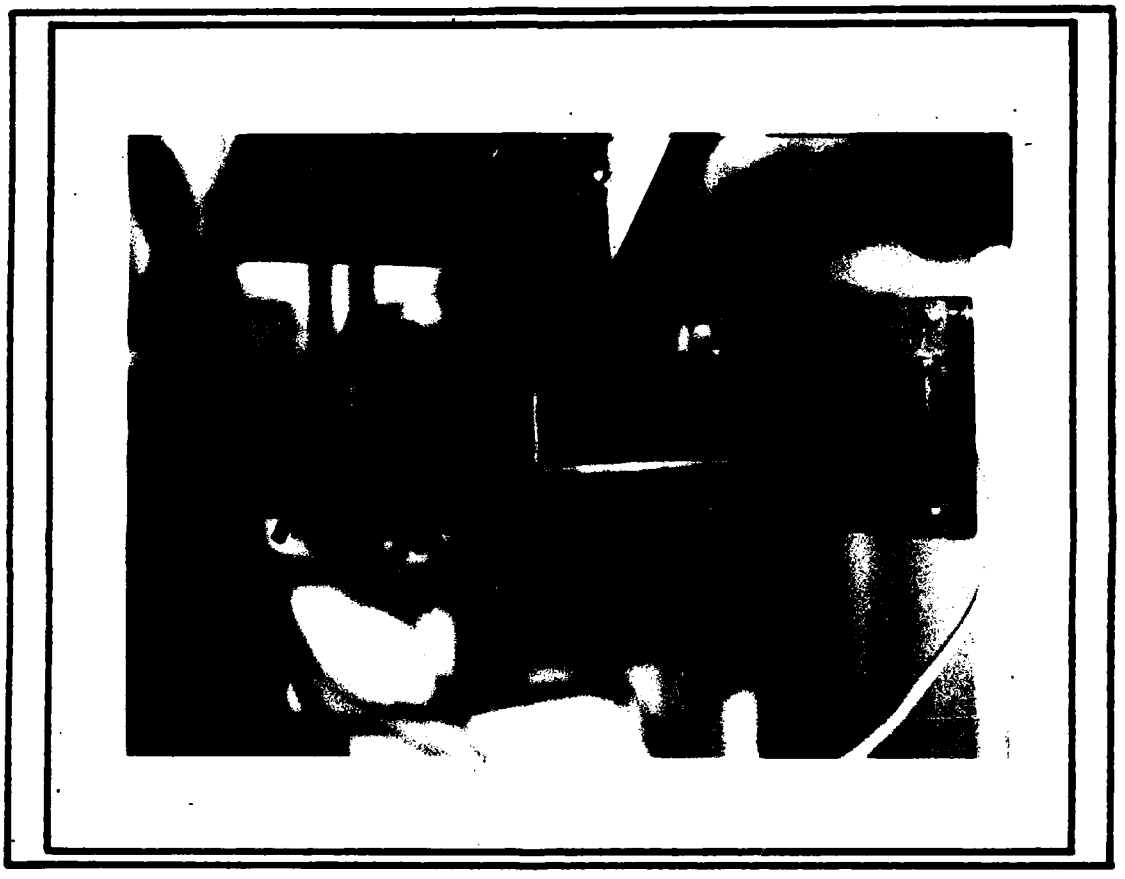

Fig. 3.1-3: test section lateral view.

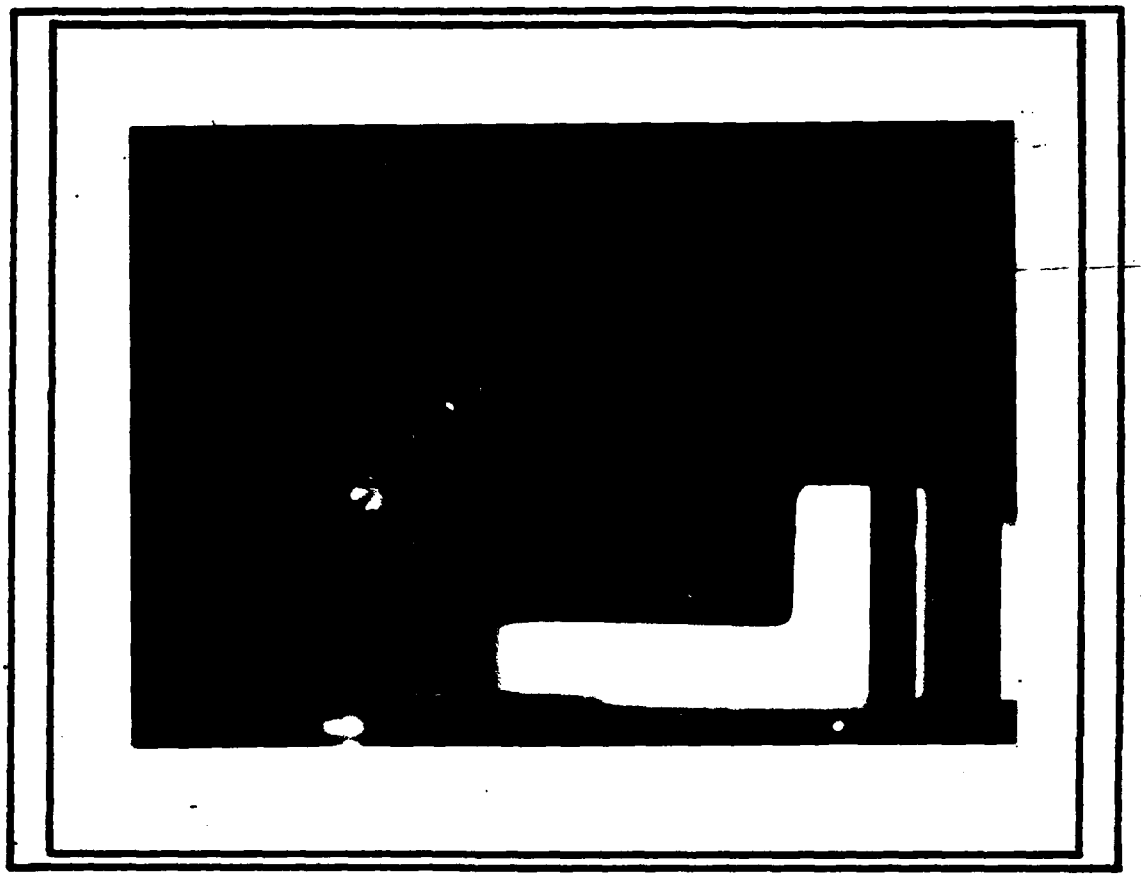

fig. 3.1-4: needle positioning mechanism.

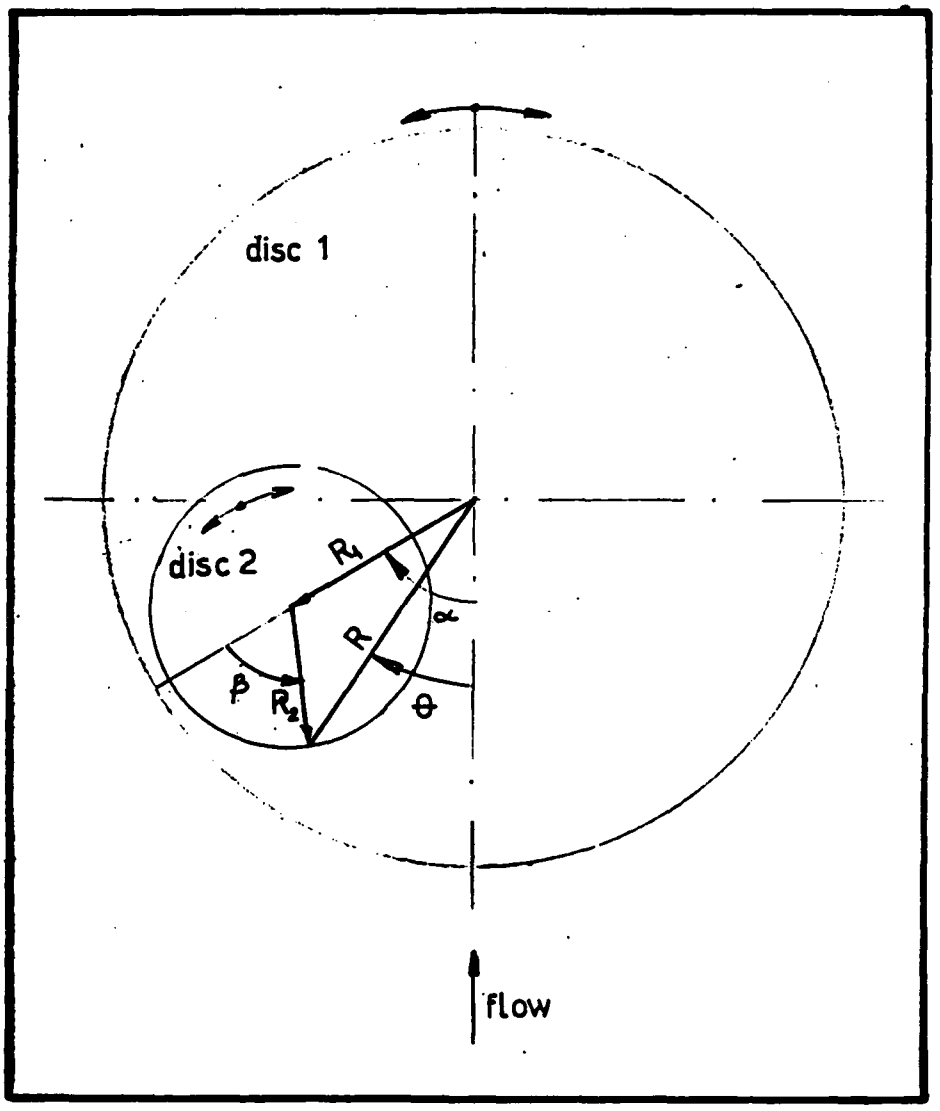

fig. 3.1-5: needle tip positioning

3.2 Seeding system.

In order to determine the characteristics of the seeding system several separate and sometimes conflicting problems had to be solved.

3.2.1. Fluorescent seed selection.

An extended literature survey has been conducted in order to find the substances fulfilling most of the requirements. The first of these was to have the emitted light intensity as high as the incident one. The second was to have a relatively large span between the maximum absorption and maximum emission wavelength in order to introduce some commercially available filters. Fig. 3.2.1.-1 [ref. 14] is illustrating these two requirements as fulfilled by a substance called Rhodamine G in ethanol (solvent).

Since we had an A_r^+ laser as light source those substances were investigated carefully which had the absorption band close to 514.5 mm - the laser beam wavelength (green). The laser can be tuned to a lower wavelength too but with a lower intensity and therefore we discarded this wavelength.

A veryuseful description of the main properties of fluorescent substances in conjunction with different solvents has been found in ref. [24], [25]. All the fluorescent (or luminescent) substances have chemical or photochemical instability which does not allow prolonged illumination or too high incident beam intensity. However the estimated parameters of our experiment are far away from the critical values (example: estimated illumination time for an air flow of 50 m/s is $4 \cdot 10^{-5}$ sec; illumination time for a rhodamine type substance to deteriorate photochemically, is several hours [26]).

Ref. [26] has proved to be most valuable since the method of illuminating the tracer substance in liquid solution droplets is essentially similar to a dye-laser system. However our conditions are far more difficult because the state of the fluorescent solution cannot be controlled in the same way [26].

The main properties of the fluorescent substances and solvents investigated are presented in tables 3.2.1. - 1. and 2. From the literature survey we selected three substances for each type (tracer and carrier) with the best (published) chararacteristics and investigated them in the laboratory. None of them is toxic and no unusual corrosion or pollution problems might occur. All are commercially available at low prices (even at high purity). No thermal restrictions were imposed on the experiments since the solvents remain in liquid state under our experimental conditions.

We determined the optimum pair (tracer/carrier) concentration for these substances (tables 3.2.1 - 1 and 2) under static conditions as described in ref. [27]. The optical set-up is shown in fig. 3.2.1-2 and the results in fig. 3.2.1.4 - 9.

The solutions were placed, at room temperature, in perspex samples (1 x 1 x 40 mm) used in spectrometry. The samples were illuminated with the A_r^+ laser tuned at 514.5 nm. A power meter indicated the input laser power. A photomultiplier was used to collect the emitted light. A filter for the incident 514.5nm beam was placed in fron tof the photomultiplier. The photomultiplier was placed under a 20^0 angle from the incident beam and focused at different distances in order to check the influence of the extinction in the third volume.

In principle the amount of light collected is different because the volume of emitting solution is different (see fig. 3.2.1 - 3). The output of the photomultiplier was connected to a digital voltmeter and the readings manually recorded.

As it can be seen in fig. 3.2.1 - 4 and 5 only small differences are due to the placement of the focus. In the weaker solutions the influence is somewhat sensible (see log μ = -5; -6).

The solutions of the tracer substances in the carrier ones (solvents) have specific properties according to the solvent and the concentration of the tracer. Dyes (in Table 3.2.1 - 1.) have a tendency to form aggregates of several molecules or with the solvent molecules (especially polar ones [28]. Such aggregates have a different absorption spectrum than single molecules. The aggregation phenomenon can be reduced by temperature increase [28]. However a temperature increase leads to a decrease in fluorescence (fig. 3.2.1 - 9) and [28].

As it can be seen in fig. 3.2.1. - 5 there is only a small difference between the output of the water solution and the ethylenglycol one (same concentration of Rhodamine 6G) although the first is a polar solvent and the second not. The aggregation is insignificant in this case. Both solutions showed good stability in time (chronometer measurements). The third solution (fluoresceine in water) appears to be more sensitive to prolonged illumination. One has to bear in mind that part of the incident beam energy converts into heat in the solution [29]. As it can easily be seen in all fig. 3.2.1 - 4,5,8 the solutions of rhodamine 6G are far more strong than the fluorescein or uranine ones. On the other hand there is no significant difference between the solvents for the rhodamine 6G solutions although there is a slight advantage for the ethylenglycol.

The most important factor to be analyzed is the concentration of tracer substance. Fig. 3.2.1 - 6,7 show that at high illumination (0.6W input power) there are no differences in output whether working at 1:4000 or at 1:10000000 !! The differences are greater at lower input powers (0.4 or 0.2 w).* At very low input (0.2w) the effect of the concentration becomes important (in ethylenglycol 1:4000 solution is responding almost twice higher than the 1:100000 solution). For

---

* Note

The fluoreacent substances have an almost directly proportional emission to the incident radiation up to a certain value when saturation occurs [29]. We can see an almost linear variation fsom 0.2+ 0.4 w input at any concentration.

Table 3.2.1. - 1.

Substance (tracer)	Chemical formula	Molecular weight kg/kmol	Solubility*			Absorptivity L/mol.cm	Best solvent for excitation	Maximum emission in ethanol
			water	eth.glyc.	ethanol			
Fluoresceine	$C_{20}H_{12}0_5$	332.3	s(pH5.8) p(pH8.1)	R-	R	$9.32 \cdot 10^4$ at 501 nm	ethanol	560 nm
Uranine	$C_{20}H_{10}O_5Na_2$	376	H+	V-	R+	$11.0 \cdot 10^4$ at 485 nm	ethanol	570 nm
Rhodamine 6G	$C_{28}H_{31}N_2O_3Cl$	479	M+	R+	R+	$10.6 \cdot 10^4$ at 530 nm	ethanol	590 nm

Table 3.2.1.-2.

Substance (carrier)	Chemical formula	Molecular weight kg/kmol	Density kg/m^3 20°C	Surface tension vs. air-dyn/cm	Viscosity cp	Refraction index	Heat of Vaporization kj/kg	Temp. of vap. °C.
Water	H_2O	14.0	1000	73.05 (18°C)	1.00	1.333	2256.2	100°
Ethanol	C_2H_6O	46.07	791	24.050°C)	1.2	1.361	855.0	78.3°
Ethylen-glycol	$C_2H_6O_2$	62.07	1080	47.7 (20°C)	5.0	1.393	800.0	196°

* Note:
Seventeen degrees of solubility are defined [25]: s = slightly soluble; p = poor;
M+ = more than 1%; slightly more than M+; R+ = very readily soluble (5-7%);
V- = slightly more than R+; H = highly soluble

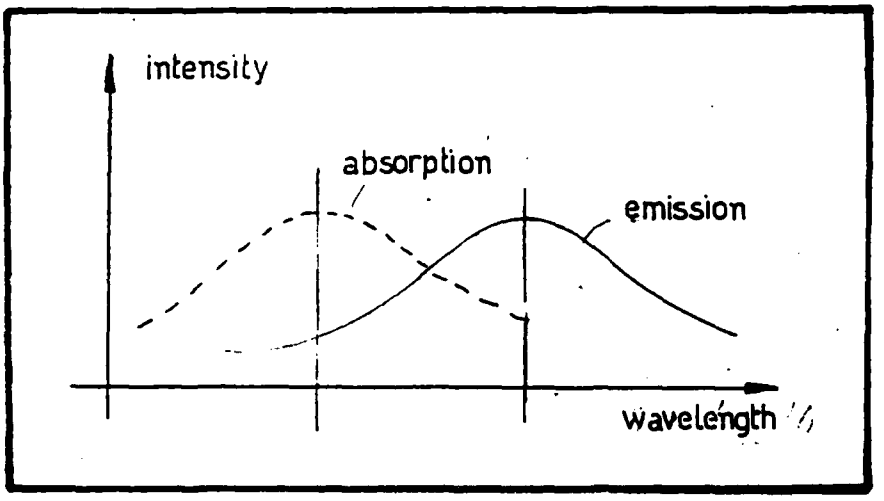

fig. 3.2.1-1: "mirror" simetry in absorbtion emission characteristic of rhodamine 6G [14]

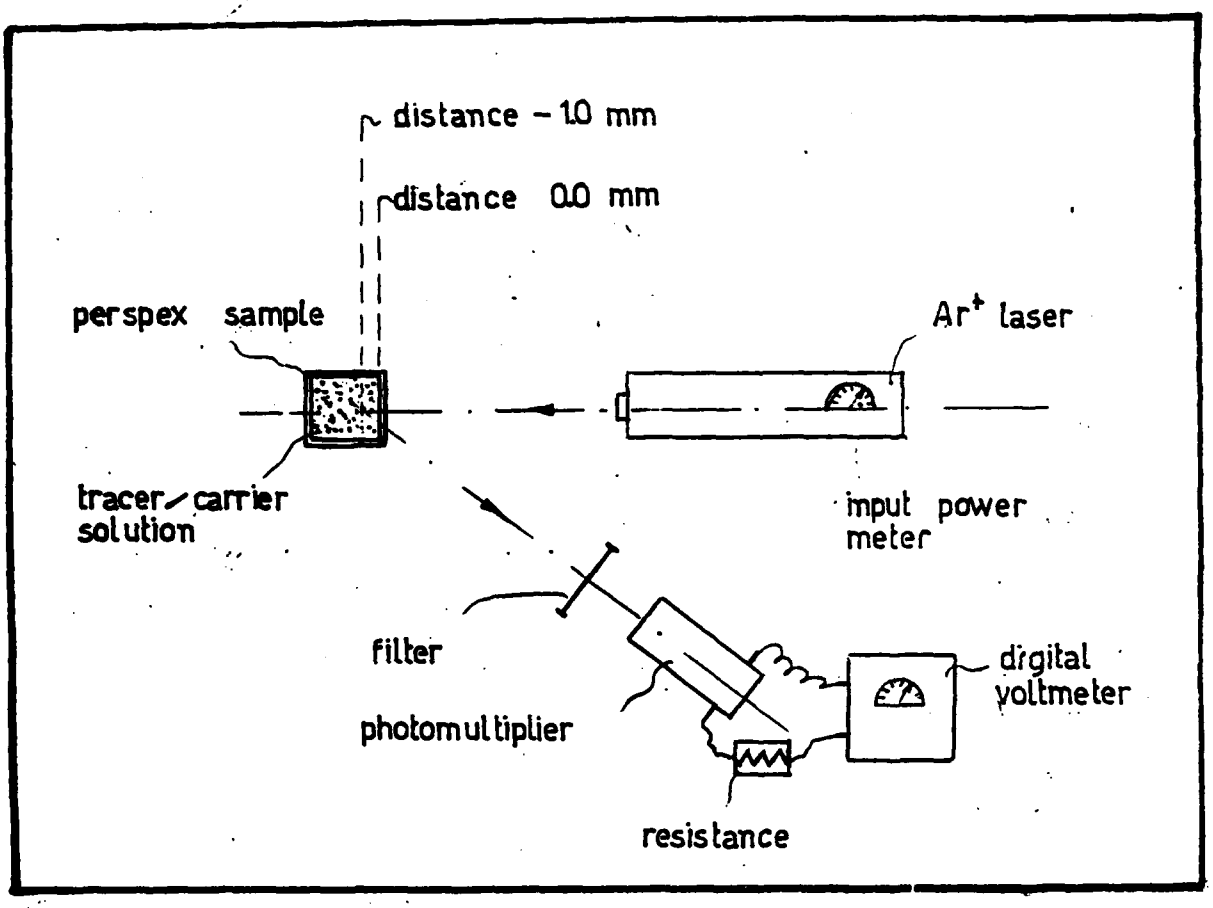

fig. 3.2.1-2: optional set up for static study of fluorescent solutions.

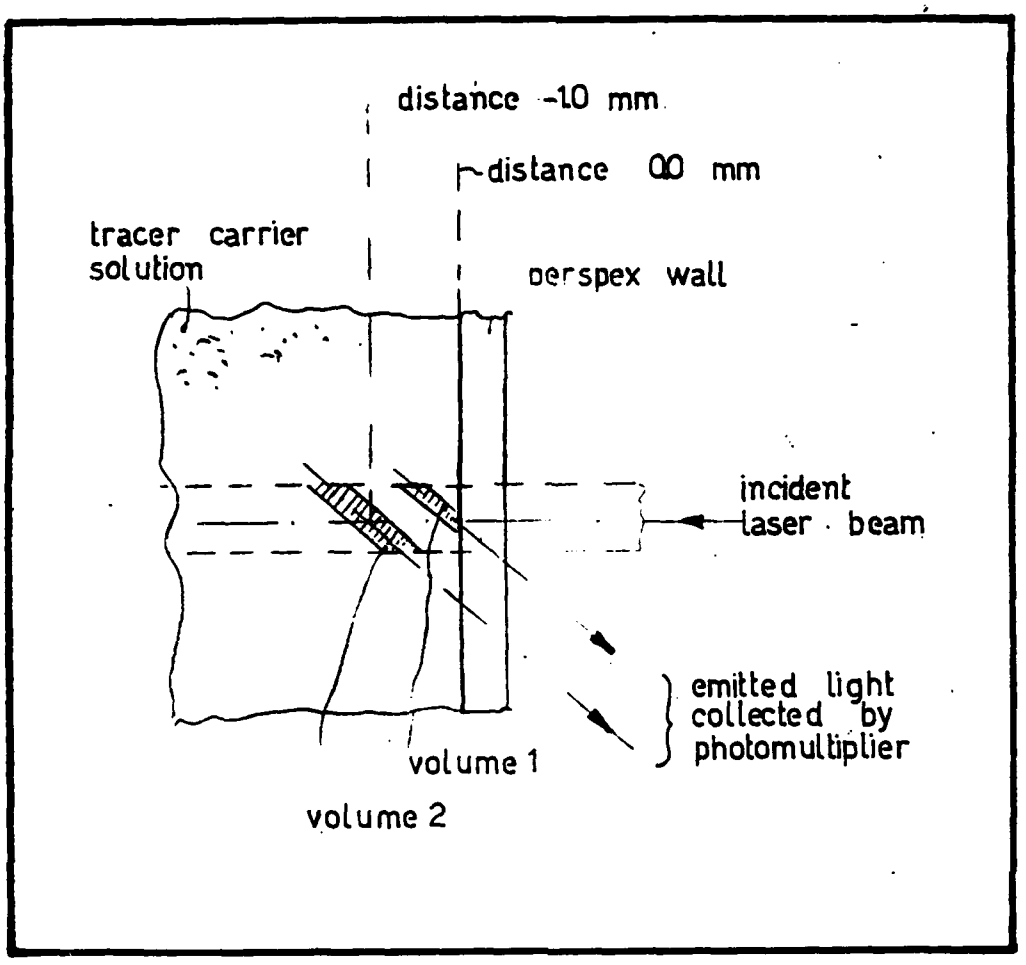

fig. 3.2.1.-3: collected light dependence on solution volume in focus of the photomultiplier lens.

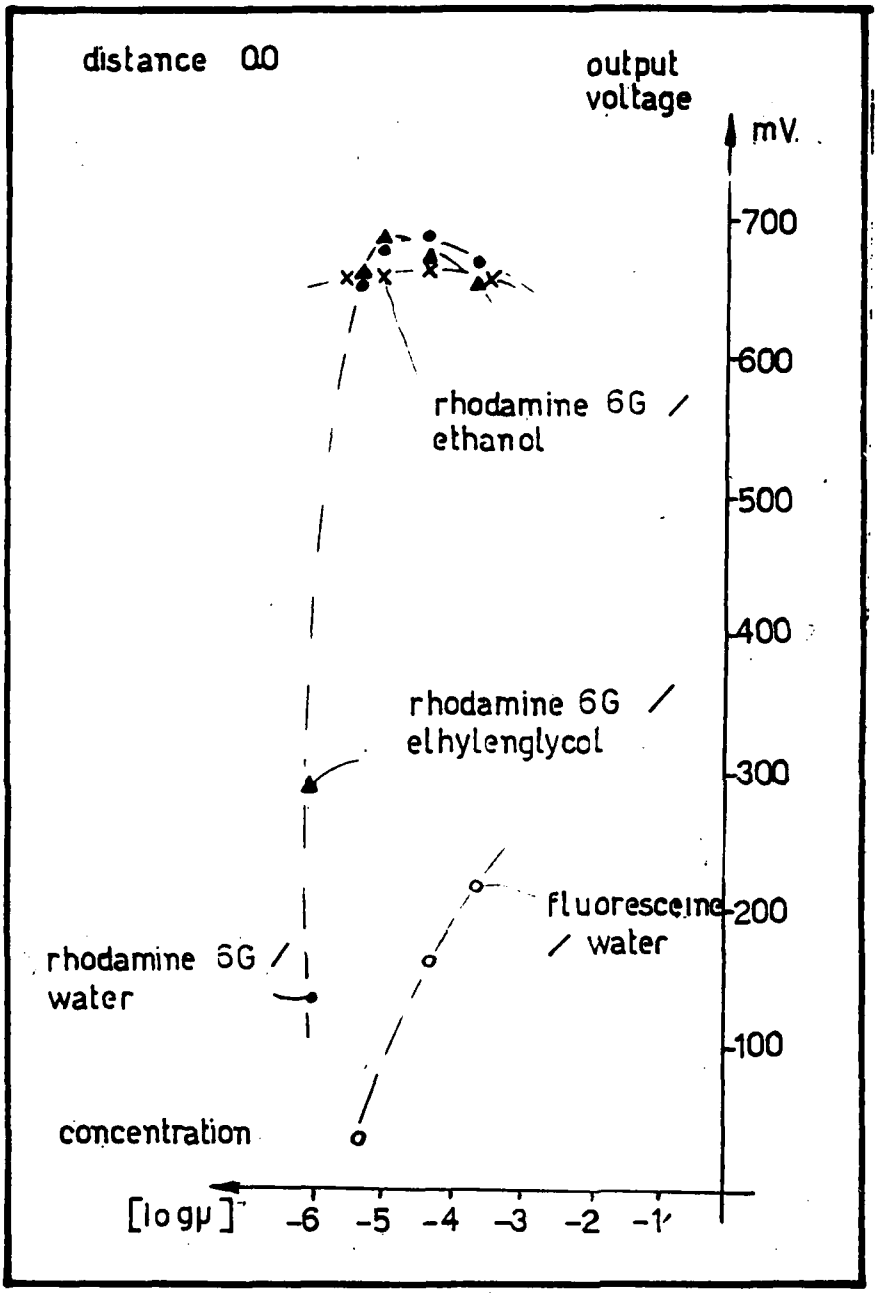

fig. 3.21.-4: output dependence on fluorescent tracer concentration

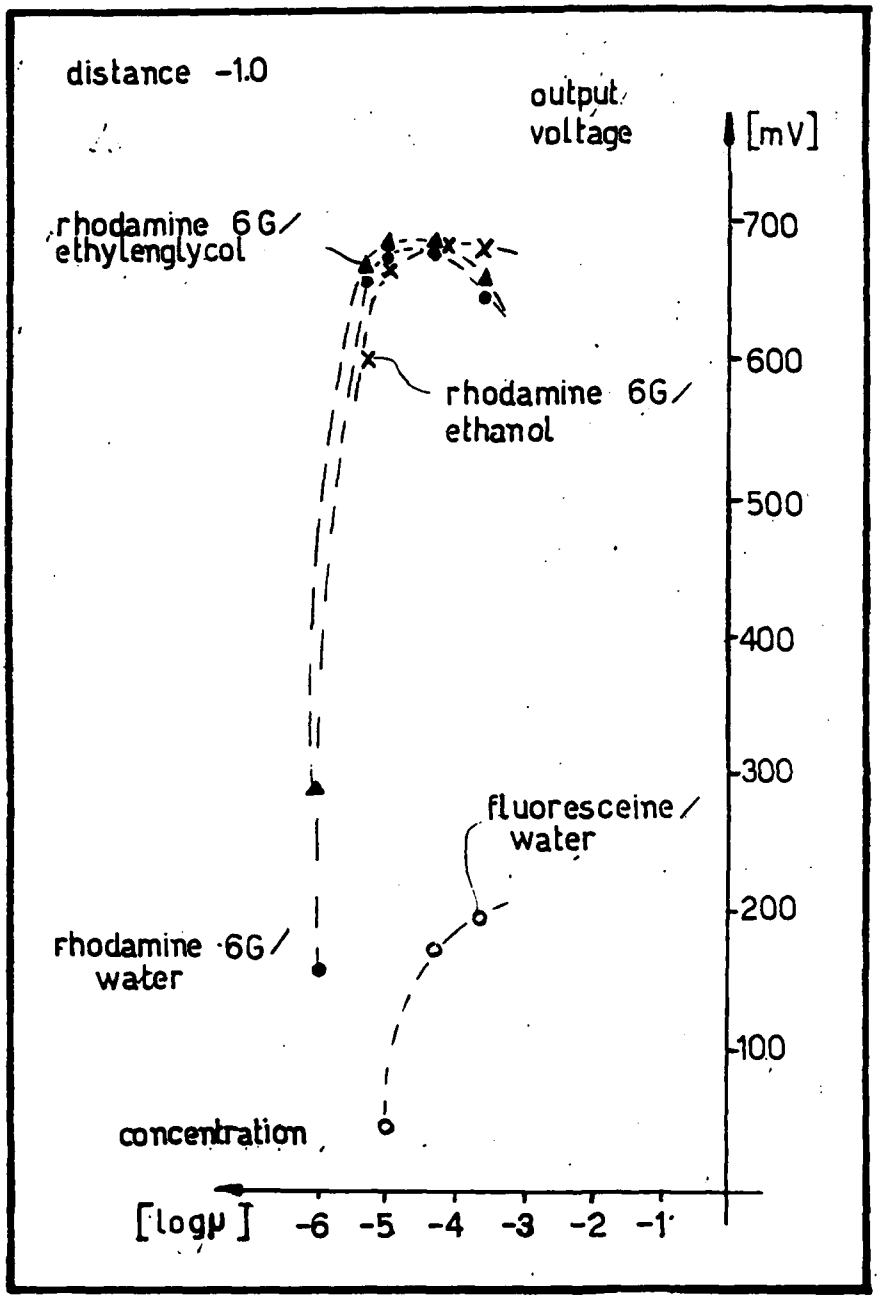

fig. 3.2.1-5: output dependence on fluorescent tracer concentration.

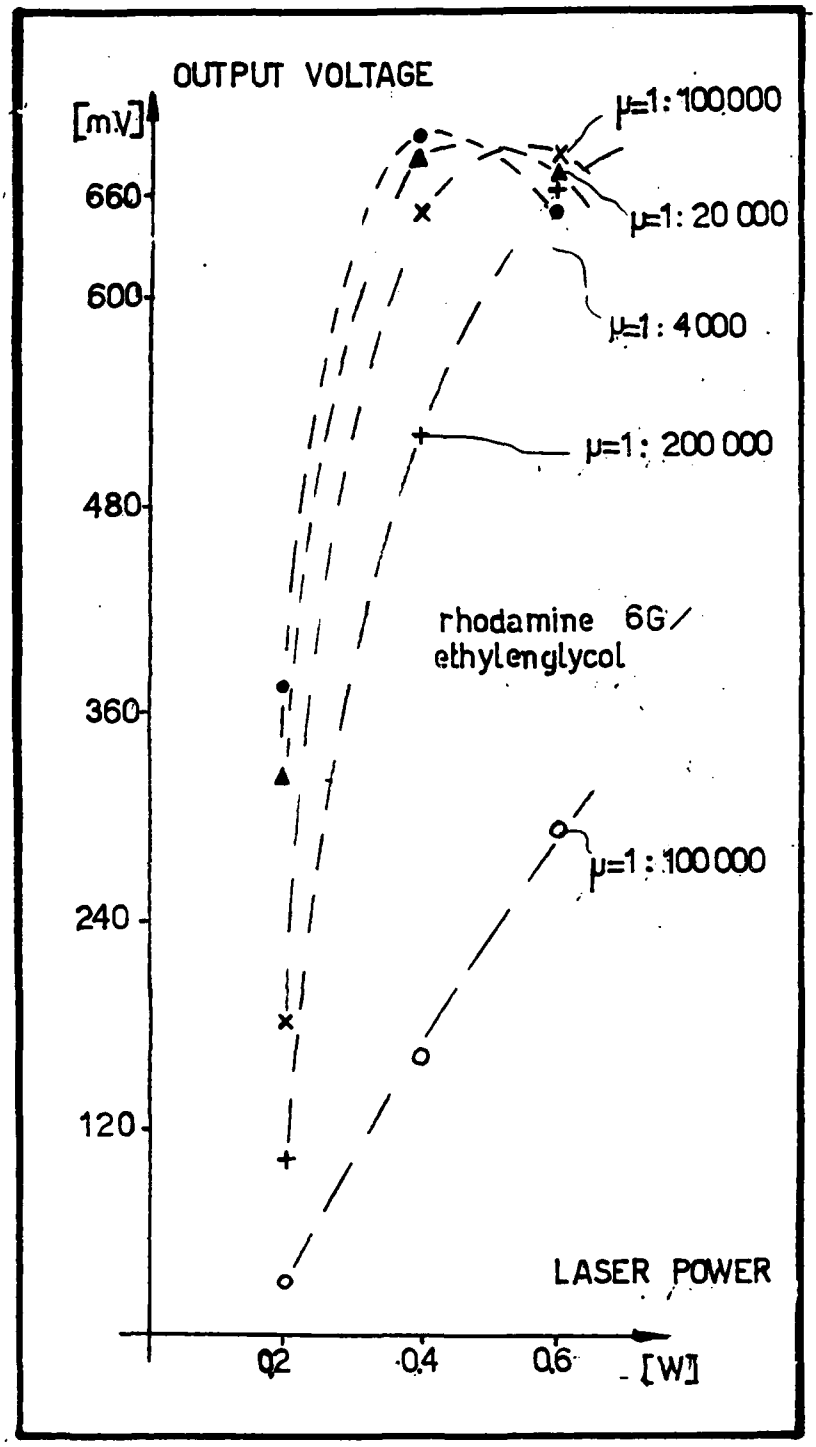

fig. 3.2.1-6: output dependence on laser power

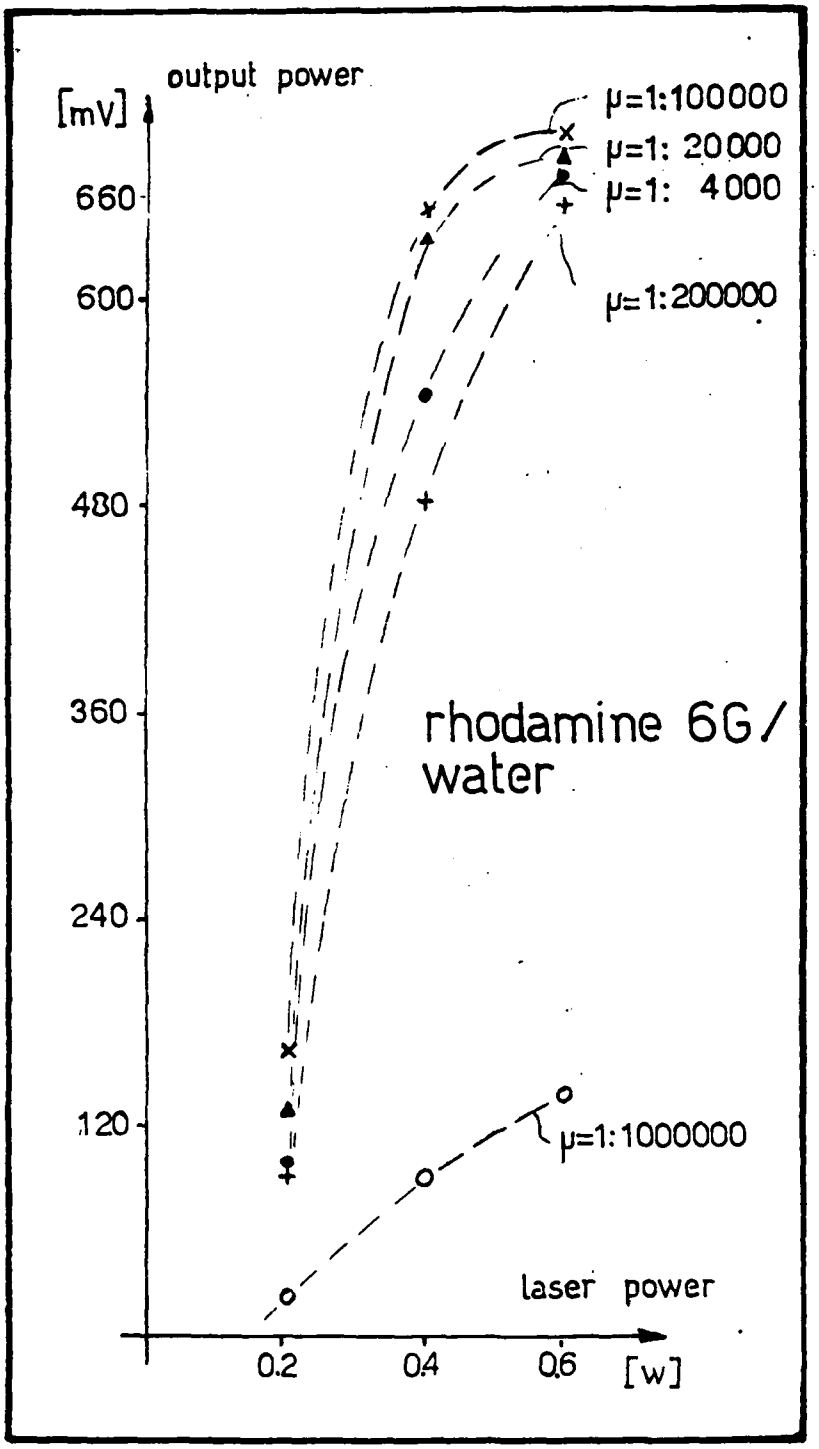

Fig. 3.2.1-7: output dependence on laser power

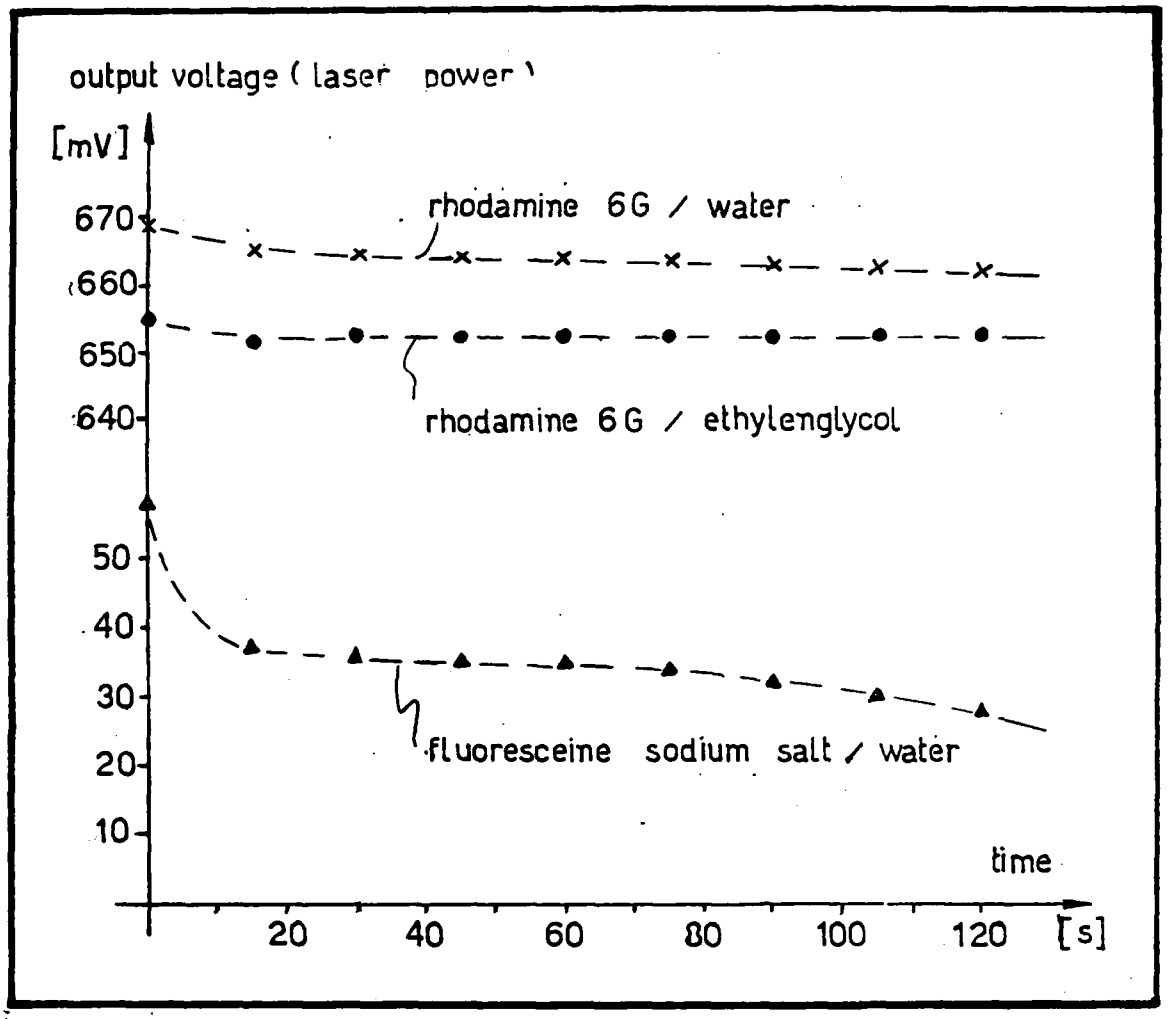

Fig. 3.2.1.8: output dependence on illumination time.

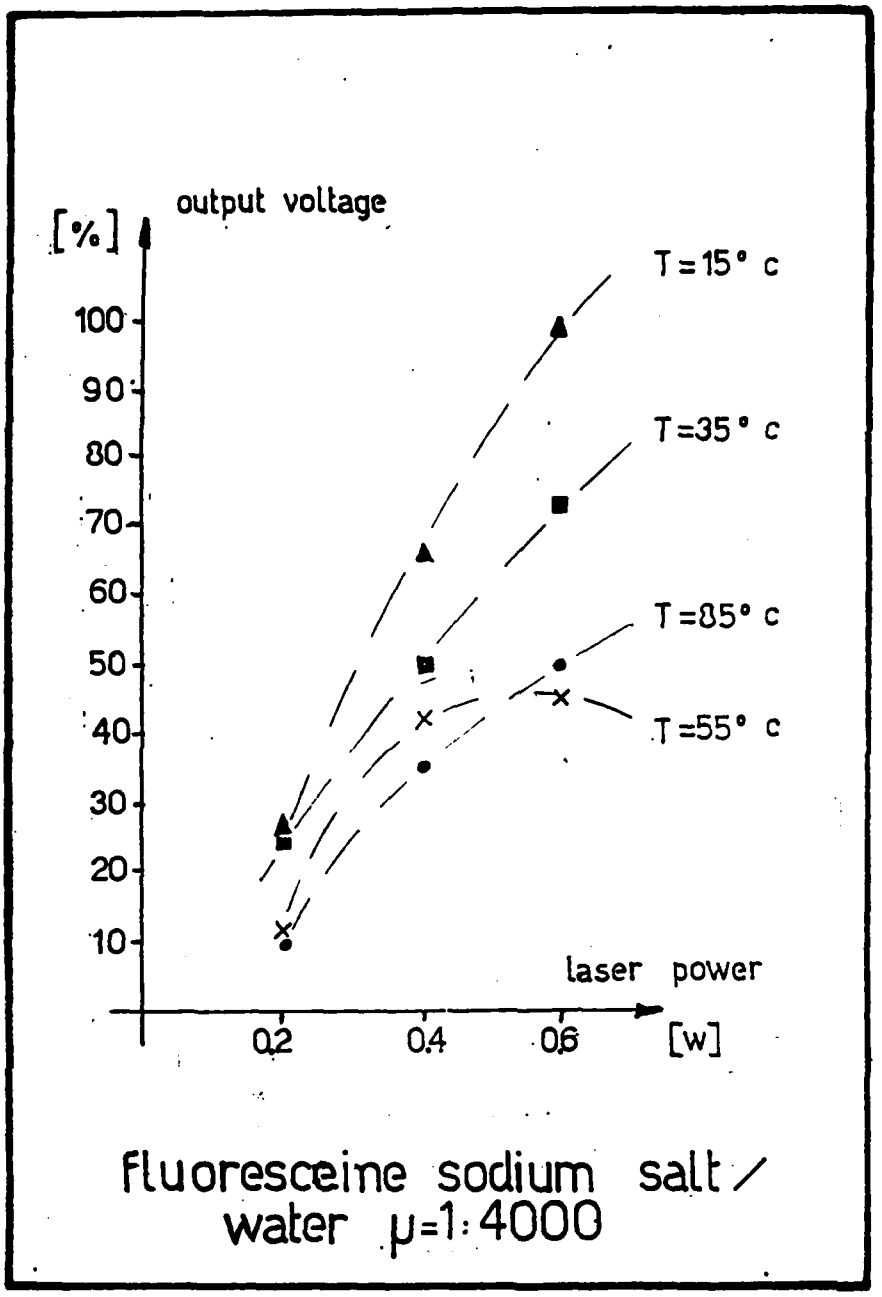

fig. 3.2.1-9: temperature influence on relative output emision.

the 0.4w input power the response in both water and ethylenglycol are similar down to 1:100000.

Our measurements were conducted in order to obtain relative absorption/emission characterstics for the substances in tables 3.2.1 - 1,2.

Our qualitative findings are in good agreement with other measurements, ref. [30], [29]. The better performance of the rhodamine solutions over the fluoresceine (uranine) ones is clearly demonstrated in fig. 118 pp. 350 ref. [30]: the rhodamine solution yields three times stronger than the fluoresceine one (see also our fig. 3.2.1 - 5). The maximum output is also found around 1:100000 [30]. Our finding that these substances are not fluorescent in crystallin format at room temperature has also been confirmed in literature. - ref. [30] pp. 448.

We have concluded that for our experiments the rhodamine 6G in water solutions with concentrations between 1:5000 to 1:200000 can be used with a predictably good performance.

3.2.2 Seeding aerodynamics.

The liquid droplets which carry the fluorescent material have to follow as closelyk as possible the velocity changes of the flowing fluid. The droplets have an inertia which grows with their diameter. On the other hand the optical parameters (incident light collected, emitted light) increase with their diameter. Therefore a compromise has to be realized between these contradictory tendencies, for the given experimental set-up. A detailed analysis is beyond the scope of this work. However a concise presentation follows based mainly on ref. [31].

The relative motion between a droplet (particle) and a surrounding fluid is expressed by the eq:

$$\frac{\pi d_p^3}{6}\cdot\rho_p\cdot\frac{dU_p}{dt}=-3\pi\cdot\mu\cdot d_p V+\frac{\pi d_p^3}{6}\rho_t\cdot\frac{dU_t}{dt}-\frac{1}{2}\cdot\frac{\pi d_p^3}{6}\cdot\rho_t\frac{dV}{dt}$$

$$-\frac{3}{2}d_p^2\sqrt{\pi\mu\rho_t}\cdot\int_o^t\frac{dv}{d\xi}\cdot\frac{d\xi}{t-\xi}$$

[Hinze, 1959]

where: dp = droplet diameter

ρ_p = droplet density

ρ_t = fluid density

μ = fluid viscosity

t = time

U_p = instantaneous droplet velocity

U_t = " fluid velocity

V = " relative velocity $(U_p - U_t)$

This eq. neglects electrostatic, gravitational and centrifugal forces. The Reynolds number for the creeping flow past a sphere is defined as:

$$Re_p = \frac{\rho_p | V | \cdot dp}{\mu} < 1$$

For the cases of liquid droplets in gas flows $\rho_p/\rho_t >> 1$ and the eq. can be simplified to:

$$\frac{dU_p}{dt} = \frac{18\mu}{\rho_p d_p^2}(u_f - u_p)$$

In the case of centrifugal flow a specific term is added:

$$\frac{dU_p}{dt} = \frac{18\mu}{\rho_p d_p^2}(u_f - u_p) + r \cdot w_r^2$$

where r = radius of curvature

w_r = angular speed

Two solutions were calculated for this eq., in simplified hypothetical, cases [30]: turbulent subsonic linear flow and forced vortex with zero radial fluid velocity. Both have shown that droplets with diameters greater than 1μm either cannot follow turbulent changes with frequencies higher than 10 KHz or will be rapidly deposited on the external cylider of the vortex flow (reach the wall after $2 \cdot r_o$ path - r_o is the radius of droplet introduction in the vortex).Similar results have been obtained in [32].

Several experimental works [33]. [21], [19] have confirmed these findings. For a droplet density of ~1g/cm^3 velocity deviations of less than 1% and angular deviations of less than 1^o can be obtained for flows with velocities up to ~400 m/s [33]. For laser-Doppler measurements performed within a compressor rotor, a 6^o angular deviation and ± 2% velocity deviations wre obtained for droplets of 1.5μm diameter.

3.2.3. Apparatus description.

Several conditions have to be fulfilled by the seeding apparatus: a) to transform the

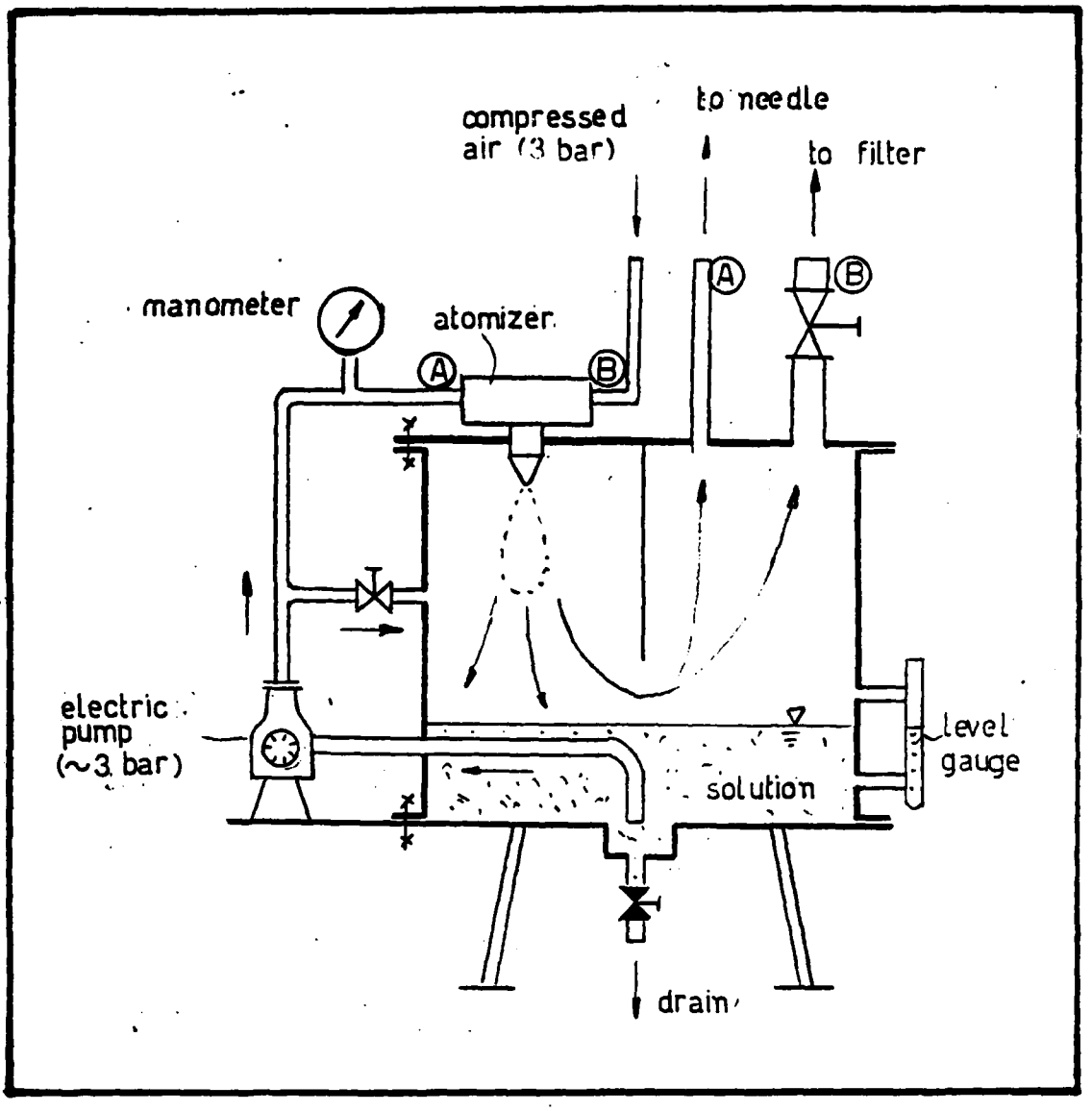

Fig. 3.2.3-1: aerosol generating unit.

tracer/carrier solution in an aerosol; b) to separate the small droplets (~1+ 5μm diameter); c) to introduce the aerosol with these droplets isokynetically in the studied area; d) to allow the continuous operation of the system.

An apparatus fulfilling these conditions has been especially built (fig. 3.2.3 - 1.) An electrically driven pump feeds the atomizer with tracer/carrier solution continuously. The pump supplies $2dm^3/min$ of liquid at 3bar. A manometer indicates the pressure at the atomizer inlet A. Compressed air is suppllied at the atomizer inlet B, from the laboratory standard air supply. A pressure rgulator maintains the air inlet pressure at 3 bar. The atomizer has a 0.,45 mm orifice for the waterjet and a final outlet diameter of 1.25 mm. Therefore a sonic air flow is obtained, in the 1.25mm orifice. This flow breaks the low velocity liquid in small droplets. The air and droplets jet is expanding freely in the vessel. This vessel has several functions: it separates the small droplets and directs the aerosol to the outlets A and B, collects the bigger droplets in its lower part and ensures the correct functioning of the pump; it ensures the change in flow at outlet B. This apparatus is of the aerodynamic dispersion type. The vessel is mobile and can be easily cleaned. A quantity of 12kg of solution is initially introduced in order to ensure a sufficient suction level for the pump. No sensible change has been observed at the level indicator after approx. 20hr of work.

According to the estimation, shown in appendix 3, the diameter of droplets introduced in the test section is lower than 10 μm.

3.3 Optical set-up

3.3.1 Optical set-up description.

The flow in turbomachines is three dimensional. Therefore we adopted a method suitable both for the two dimensional flow in our wind tunnel and the more general case - three dimensional. The method is called tomographic: the flow is "cut" by light sheets in two directions (perpendicular) [34], [40]. The tracers are photographically recorded at 90^o to the two directions. Two projections of their streamlines are obtained and the real streamlines can be reconstructed. The principal elements of the set-up and their arrangement are shown in fig. 3.3.1 - 1.

The first optical elements are the light sheet generating lenses. The laser beam is ellipsoidal and slightly divergent. In order to obtain a light sheet two methods are possible [35]: either using cylindrical lenses (or even a glass rod) or a scanning device which moves the laser beam at high frequency in one direction. The method with lenses is simpler to realize but the energy is not uniformly distributed in the section of the sheet which is of unequal width (elliptic). On the other hand the scanning devices which eliminate this inconvencience might produce stroboscopic effects and "cause important recording difficulties for exposure times only slightly different from the sweep period" [34]. We decided that for our experiment the cylindrical lenses might be sufficient.

In order to have the maximum collecting angle we placed the light collecting elements at

90° from the light sheet axis. These elements are: a filter for the laser beam wave length, a focusing lense, an image intensifier and a photographic apparatus. The image intensifier has been thought necessary in order to allow the reduction of the emitting zone (aerosol jet intersection with the light sheet) as much as possible.

The positioning mechanism allows the collecting optical system to follow the light sheet in its progression in the flow.

The filter allows only the tracer emitted light sections of the aerosol jet* coming out from the needle. In the arrangement shown in fig. 3.3 - 1. the z-z axis integrated light gives the theoretical image shown in the detail. The coordinates of the point on the streamline can be determined as shown in fig. 3.3.1 - 2. Because of specific laboratory conditions slight modifications in the placement of the equipment were made as shown in fig. 3.3.1 - 3.

The collecting optics have been positioned such as to move simultaneously with the scanning device (mirror 1) of the light sheet (i.e. the axis of the image intensifier corresponds to the axis of the light sheet and move in the same direction x - x). The up-and-down motion of the image intensifier allows for the scanning of the second direction (y - y).

A special set of alignement procedures have been elaborated for this set-up (appendix 4). These procedures enabled us to obtain the correct positioning of mirrors, lenses, a.s.o. relative to each other and the studied flow region.

---

*Note:

If the aerosol is coming out at exactly the same velocity as the fluid (air) then the notion "jet" is not appropriate.

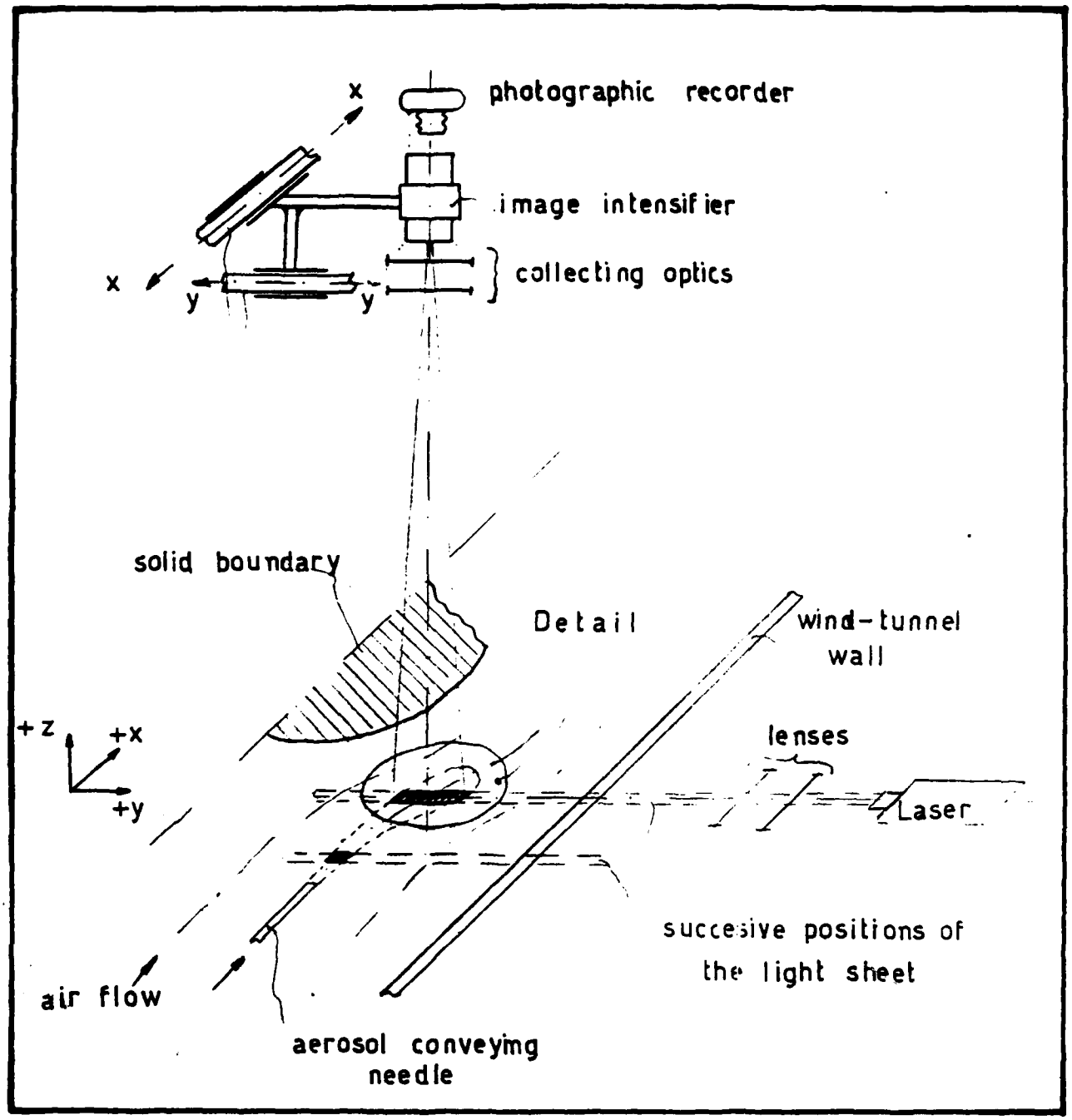

fig. 3.3.1-1: optical set-up for a two-dimensional flow visualization in a wind tunnel

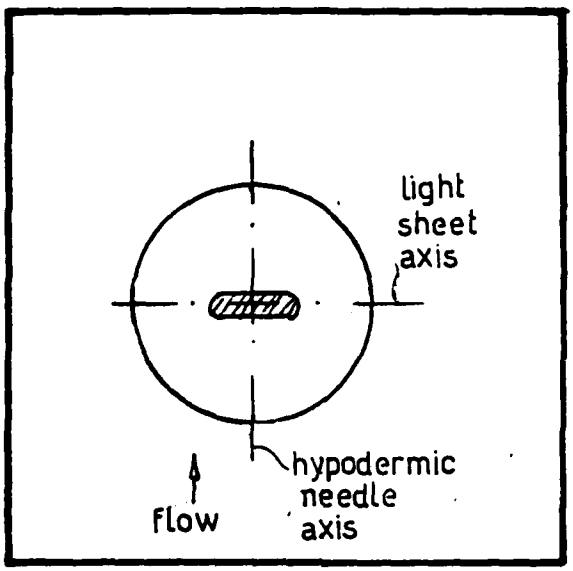

fig. 3.3.1-1: detail: image seen by light collecting optics.

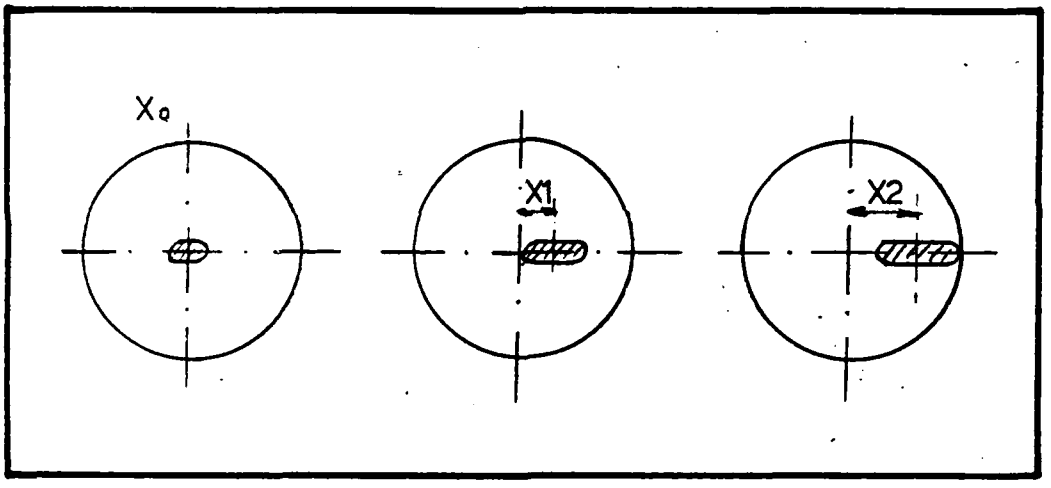

fig. 3.3.1-2: streamline axis location in picture.

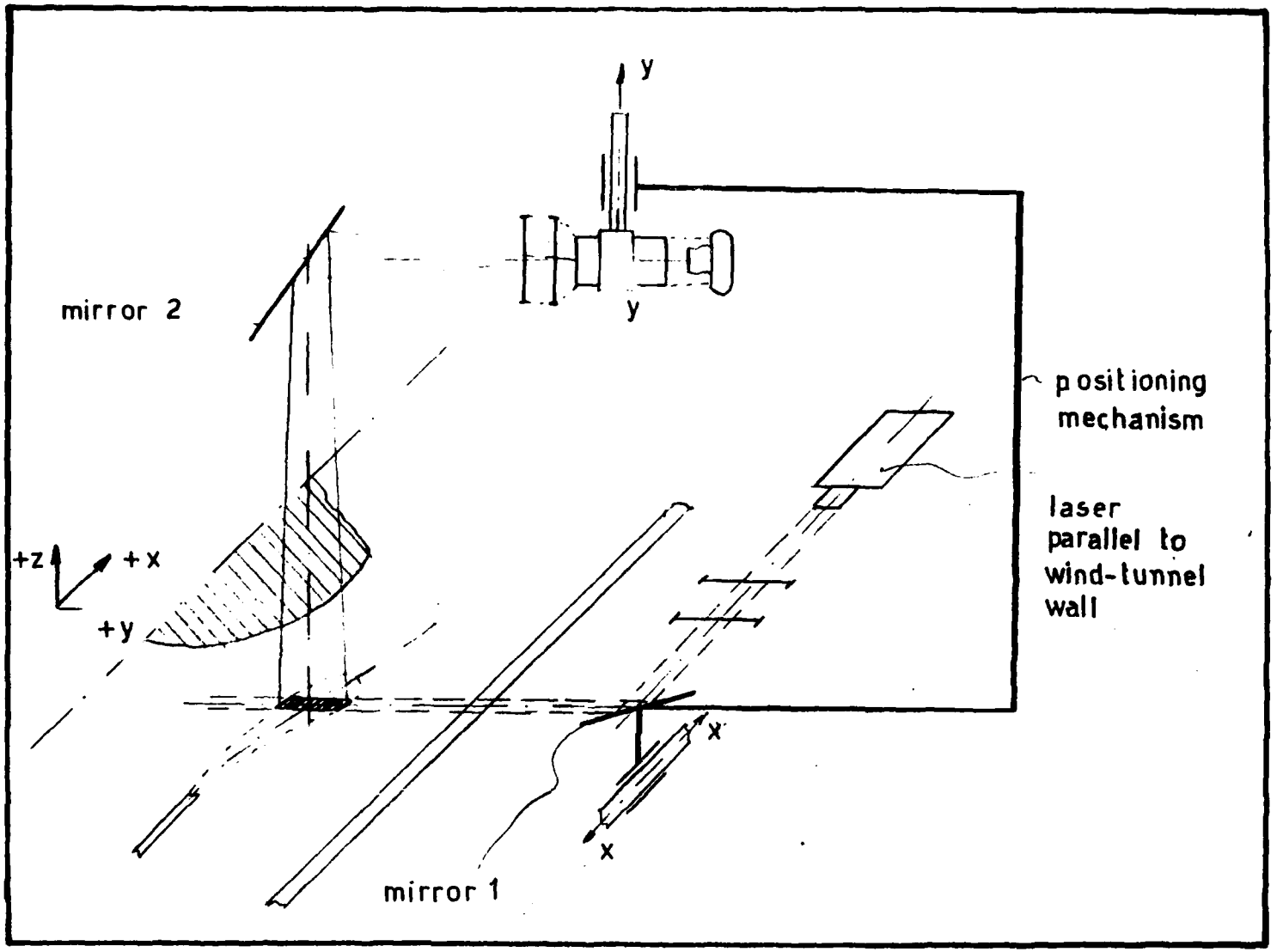

fig. 3.3.1-3: modified optical set-up using two mirrors.

3.3.2 Incident light analysis.

The light source is an Argon-ion laser (Spectra Physics model 165). It can work continuously with a power or 1w. It can work either on the blue line (488nm) or on the green one (514.5nm). The laser beam has a diameter of 1.25nm, with a divergence of 10^{-3} rad. For our experimetns the green line was used. A system of two cyindrical lenses was used to obtaln the light sheet. A spherical lens, before the two cylindrical ones, allows the reduction of the thickness of the sheet from 1.25 mm to 0.5mm [39]. The parameters of the lenses are listed in table 3.3.2 - 1.

Type	Focal length mm
spherical	250
cylindrical	44
cylindrical	44

Table 3.3.2 - 1.

If the system uses only the two cylindrical lenses the theoretical height of the sheet is equal to theincident beam diameter (1.25mm). The spherical lens raises this height to 2.5mm in the test section. The incident sheet radiance is $0.8 \cdot 10^8$ (w/cm^2 ster)

$$\text{Radiance} = \frac{\text{Power}}{\text{Test section area} \cdot \text{Divergence}^2} = \frac{1\text{w}}{1.2 \cdot 10^{-4}\text{cm}^2(10^{-2})^2} = 0.8 \cdot 10^8\left[\frac{\text{w}}{\text{cm}^2\text{ster}}\right]$$

3.3.3 Collected light analysis.

The estimate of the collected light is essential for the design of the collecting optics and photographic equipment. The problem of light absorption by aerosols of liquid droplets is fairly complicated. However a simplified calculation can give us a satisfactory estimate too [35], [36], [27], [29].

We applied twice the Lambert-de Beer law which gives the relation between incident and emerging light intensities* when traversing a solution:

---

* Note

In our case intensities have to be replaced by radiances [w/sr·cm^2].

$$I_{emerging} = I_{incident} \cdot e^{-K.c.L}$$

where:

K = extinction coefficient

c = concentration of solute (particles in suspension)

L = length of light pass

In the first stage we estimated the light absorbed by a mist of droplets. Several simplifying (but generally accepted in literature) hypothesis were made:

a. Extinction in air was neglected.

b. The reciprocal influence of droplets was neglected.

c. Only cylindrical lenses are used to generate the light sheet.

d.The mist (aerosol) is formed of 1μm diameter droplets.

e. The aerosol occupied zone has a $1 \cdot 10^{-4}$m width.

f. The droplet concentration was taken 10^{11} (droplets/m^3).

g. The efficiency factor for a rain drop [35] was 3.

The extinction coefficient is then calculated [35]:

$$K = 3 \cdot \pi \cdot d^2$$

where d is the droplet diameter.

The result of this calculation gave the amount of light absorbed in the aerosol mist:

$$I_{abs} = I_{incident} \cdot (1-e^{-k.c.L}) = I_{incident} \cdot 2 \cdot 10^{-7}$$

In the second stage we estimated the light absorbed by the tracer molecules dissolved in the carrier droplets. The hypothesis adopted were:

a. The extinction coefficient for Rhodamine 6G is $6500 \frac{1}{m \cdot mol/m^3}$ [25]

c. The droplet diameter is 1μm.

The incident light beeing the absorbed one from the previous stage we obtained:

$$I^*_{abs} = I^*_{incident} (1-e^{-k^*c^*L}) = I_{incident} \cdot 2 \cdot 10^{-7} \cdot 0.9 = 1.8 \cdot 10^{-7} \cdot I_{incident}$$

However not all the absorbved light energy is re-emitted by the tracers substance. The quantum yield (for all the investigated substances) is to be taken into account.
For Rhodamine 6G it is 0.95.
If we take into acocunt the receiving optics (i.e. a magnification of 1 with a lens of 150 mm focal length) including a filter for the laser beam (λ= 514.5mm) with a transmission coefficient of 0.8 [37] then the collected intensity of the emitted light (λ = 590 nm) is:

$$I_{collected} = I^*_{abs} \cdot 0.8 \cdot 0.05 \cdot 10^{-2} \quad [w / cm^2]$$
$$= 1.4 \cdot 10^{-9} \cdot I_{incident}$$

Using the calculation method presented in [27] we obtained roughly the same result ($2.4 \cdot 10^{-10} \cdot I_{incident}$). On the other hand a ratio of $6 \cdot 10^{-9}$ between incident and emitted light has been obtained for somewhat close conditions in [6].

The very small ratio makes a direct recording (photography) impossible, therefore a light intensifier device is justified.

We used an image intensifier with a typical 45000 gain (amplification) [38]. An intensity of $6.3 \cdot 10^{-5}$ (w/cm^2) can be expected at the photographic recorder. We may note that this is equivalent to a 4.4 μ/x illumination which is much higher than the 0.2 μ/x equivalent background illumination of the intensifier device. This will ensure a good contrast on the photography, too.

A note for the magnifying lens: the 1 x magnification with a 250 mm focal length and aperture = 5 gives a depth of field of ~13 mm (far bigger than the investigated zone ~ 1mm) [39]

$$\text{depth of field} = \frac{2 \cdot \text{focal length} \cdot (\text{magnification} + 1) \cdot \text{aperture}}{100 \cdot \text{magnification}^2}$$

3.3.4. Photographic recording.

An Olympus OM-10 apparatus equipped with a zoom lens has been used to photograph the image on the image intensifier screen. The screen is in the green colour and the recording has been made in colour, on an ASA100 Kodak film. The exposure time has been fixed at 1/2 sec. Fi.g. 3.3.4-1. shows such a photography. In order to obtain a better view, the original pictures were magnified on black and white copies.

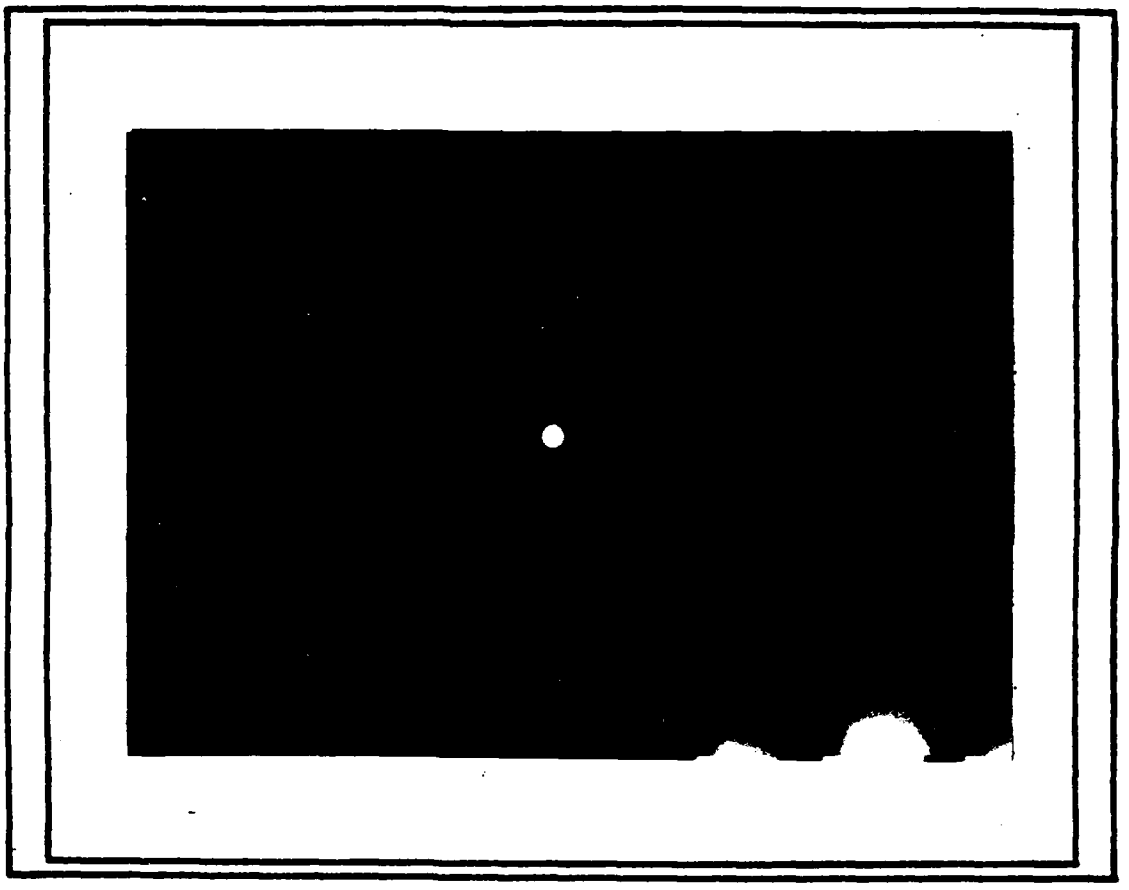

Fig. 3.3.4.-1: typical picture of the image-intensifier screen.

4. RESULTS

4.1 Description of photographic records.

The pictures in fig. 4.1.1 to 4 represent a set obtained in the same conditions. We recall that the average velocity in the free section of the wind tunnel is 5o m/s and that the water droplets were seeded with rhodamine 6G illuminated in the test section by a green laser light sheet. The emitted light is in the orange domain. The original pictures were taken in colour, the pictures in fig. 4.1.1 to 4 are magnified 4 times versions. Three bright spots can be seen distinctly.

a. The first (in the right side) represents a droplet hanging on the lip of the hypodermic needle. This droplet is almost always present. It is not directly illuminted by the laser sheet however the absorbed light is sufficient to allow a strong emission. The droplet is approximately 1-2 mm in diameter.

b. The second bright spot appears in the middle of the picture and represents the region of the aerosol jet illuminated by the laser sheet. This spot has an elliptic form growing from fig. 4.1.-1 to 4. This growth in the y-y direction is due to the jet divergence.

c. The third spot is due to light reflection by the cylinder wall. This reflection is due to slight misalignment as can be seen in fig. 4.1.-5.

The cylinder has been covered with reflecting coating but some light is still reaching the collecting optics. One must remember that the filter does not eliminate the incident wavelength 514.5 light totally but only in 80-90%.

4.2. Streamline visualization-validation.

The ultimate check of the method consists in "building" a streamline from the coordinates of points on the pictures. We compared (in table 4.2.-1.) the values of the coordinates of the axis of the second bright spot (in the middle) in fig. 4.1.-1-4 and the coordinates of the streamline points starting from the needle tip coordinates (x_o,y_o) as calculated from the inviscid flow stream function equation, ref. [41].

$$\psi / u_{\infty} = r \cdot \sin\theta \cdot \left(1 - \frac{a^2}{r^2}\right) = y\left(1 - \frac{a^2}{x^2 + y^2}\right)$$

eq. 4.2.1

where:

ψ = stream function

u_{∞} = undisturbed flow velocity

a = cylinder radius

x,y = point coordinates on the streamline

table 4.2.-1.

Y mm	x mm	Xcalc mm	δx %
18.6	-32.9	-34.9	~ 6
20.4	-31.1	-34.0	~ 8.5
22.2	-29.3	-33.0	~ 11.2
24.0	-27.5	-32.0	~ 14.0

X_0 = -34.7mm

Y_0 = 18.6 mm

a = 30.mm

The value of ψ/u_∞ is calculated from the same equation for $x = x_0$ and $y = y_0$.

The coordinates of the points on the pictures were manualy measured.

It can be seen easily that at the last point photographed on the same jet (fig. 4.1.4) the error in determination is of approx. 15%. Such a value can be considered very encouraging at this stage of the experimental method development.

4.3. Conclusions

The first conclusion to be drawn is that a method of visualization based on laser induced fluorescence is feasible under conditions close to those in turbomachines.

However atractive, one has to have in mind that a tracer of the seeded droplet type implies very complicated problems in the seeding apparatus (design, control, flexibility, a.s.o.) which has to be specially designed for the experiment.

The optical problems are rather easy to overcome with the equipment available today (lenses, filters, image intensifiers, a.s.o.) but a special attention has to be given to the positioning mechanisms both of the needle and the optical set-up. These mechanisms have to be of very high precision when complicated flows are to be investigated.

In order to determine the applicability boundaries of the method further refinements and trials are necessary.

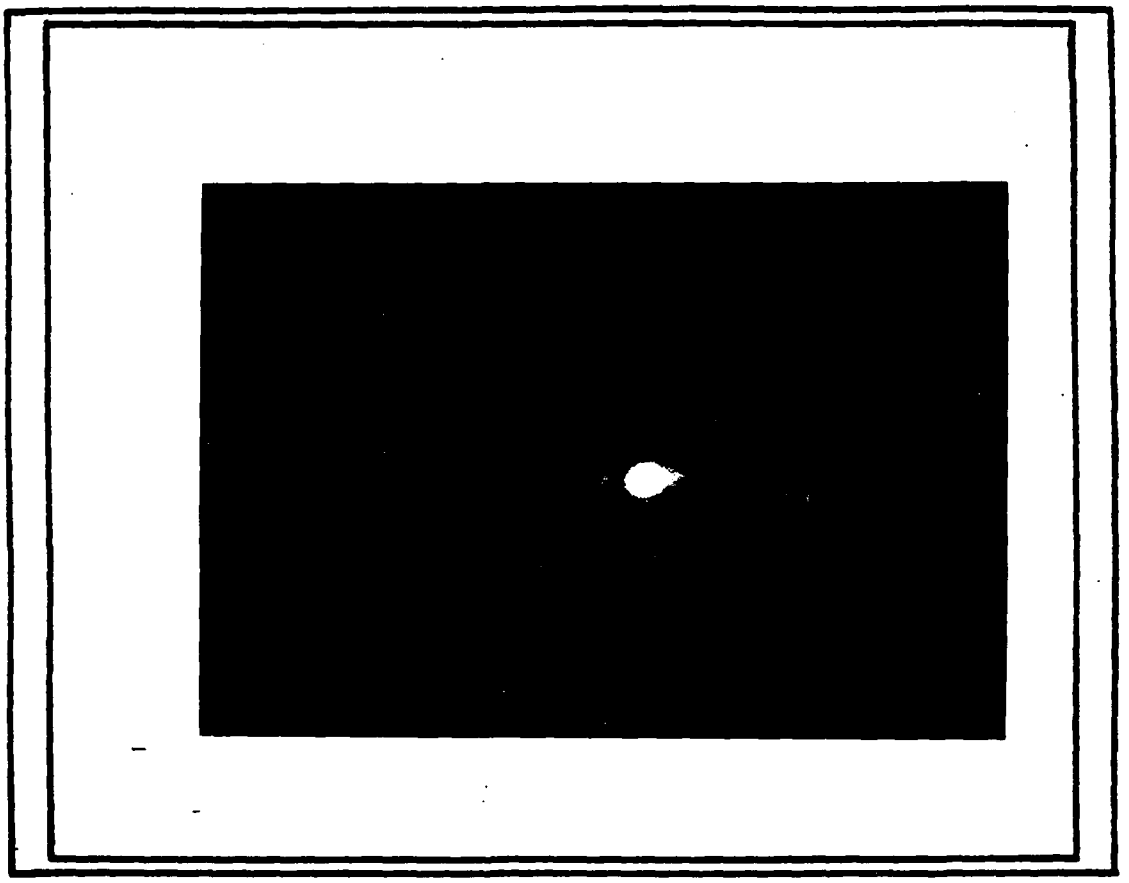

fig. 4.1-1: streamline visualization
step 1

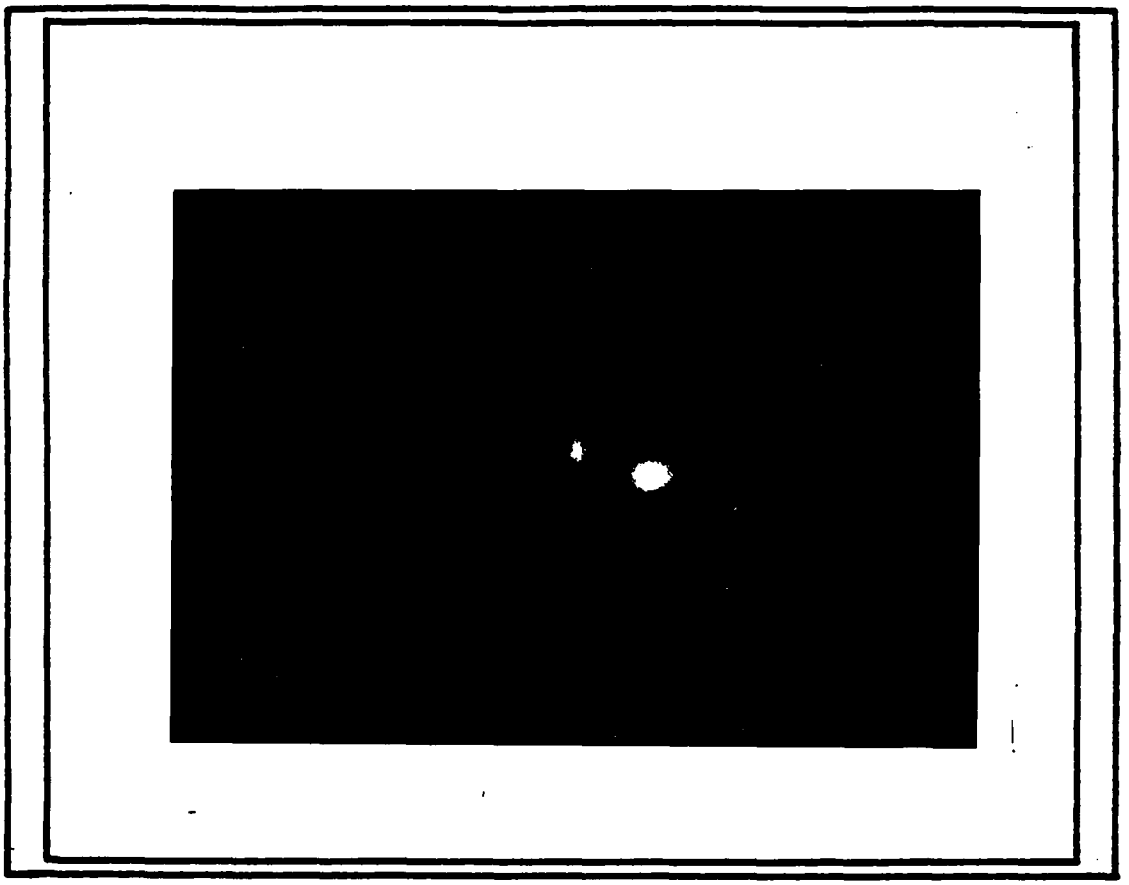

fig. 4.1-2: streamline visualization step 2

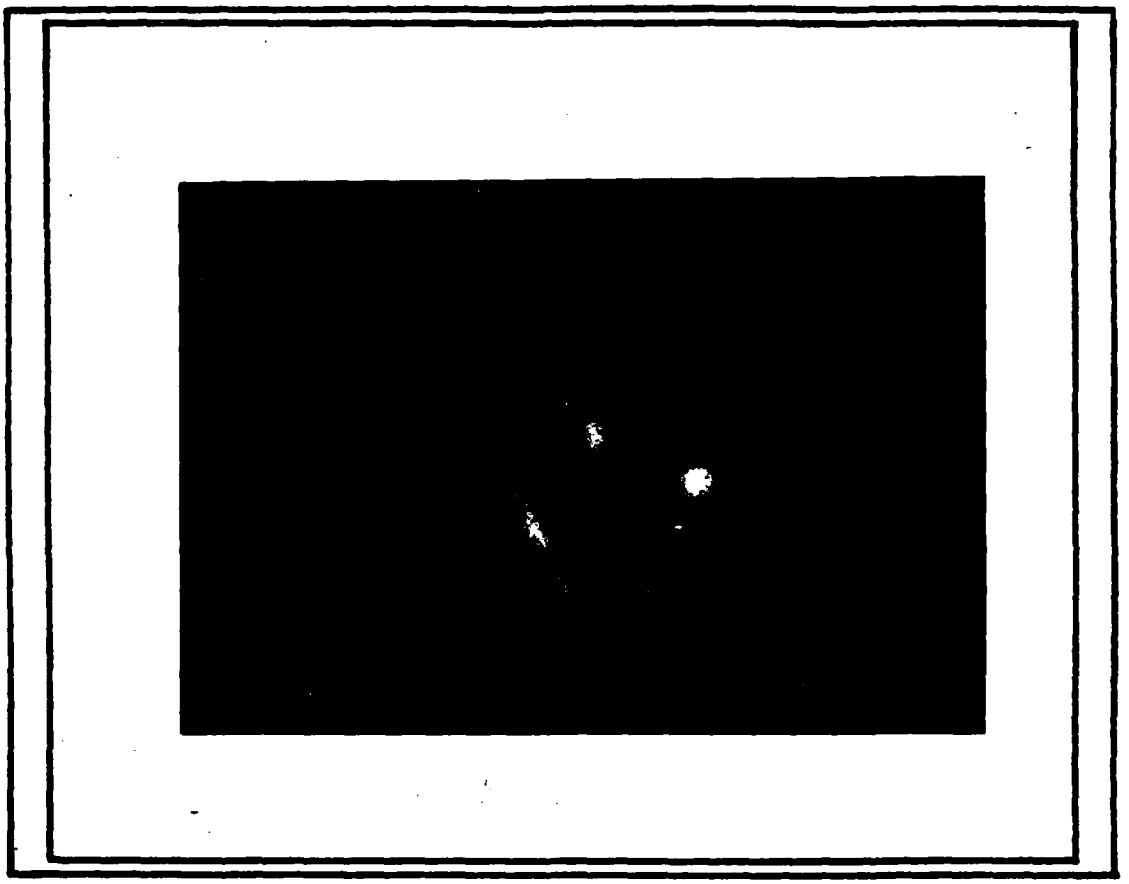

fig. 4.1-3: streamline visualisation step 3.

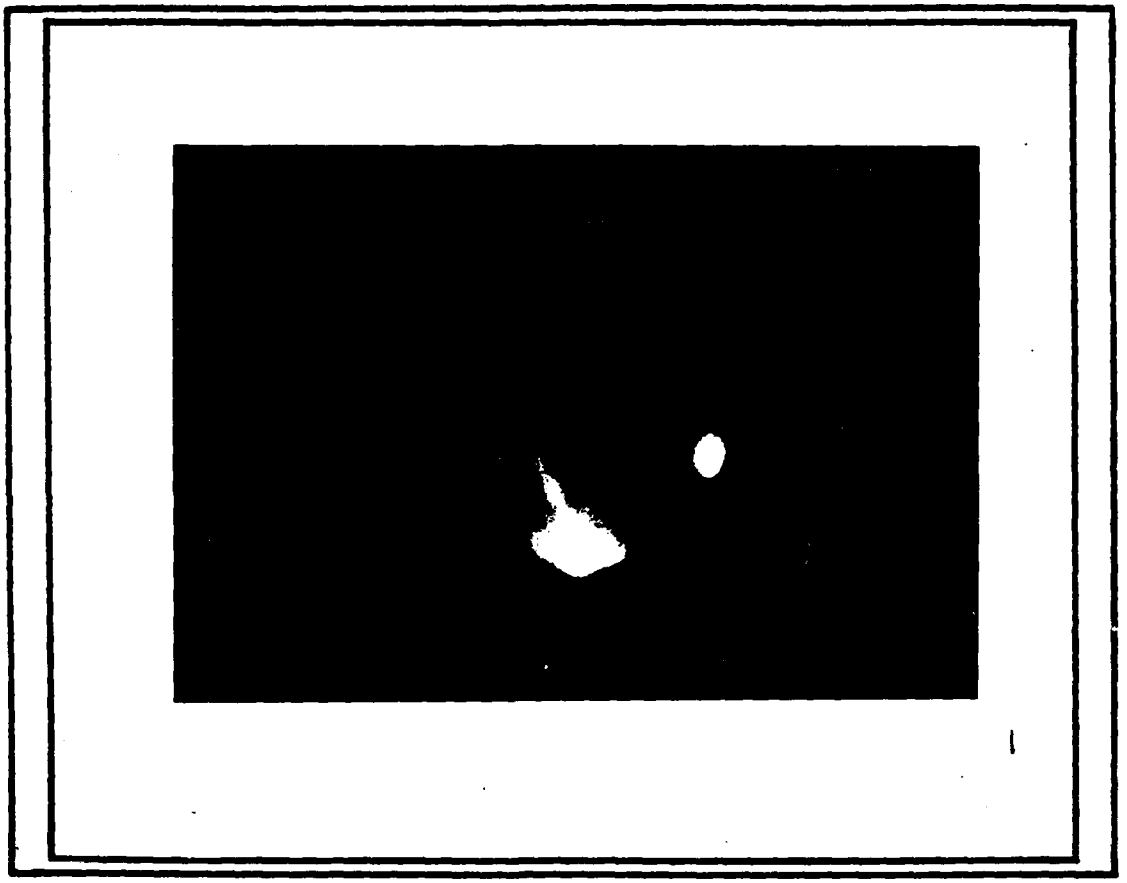

fig. 4.1-4: streamline visualization
step 4

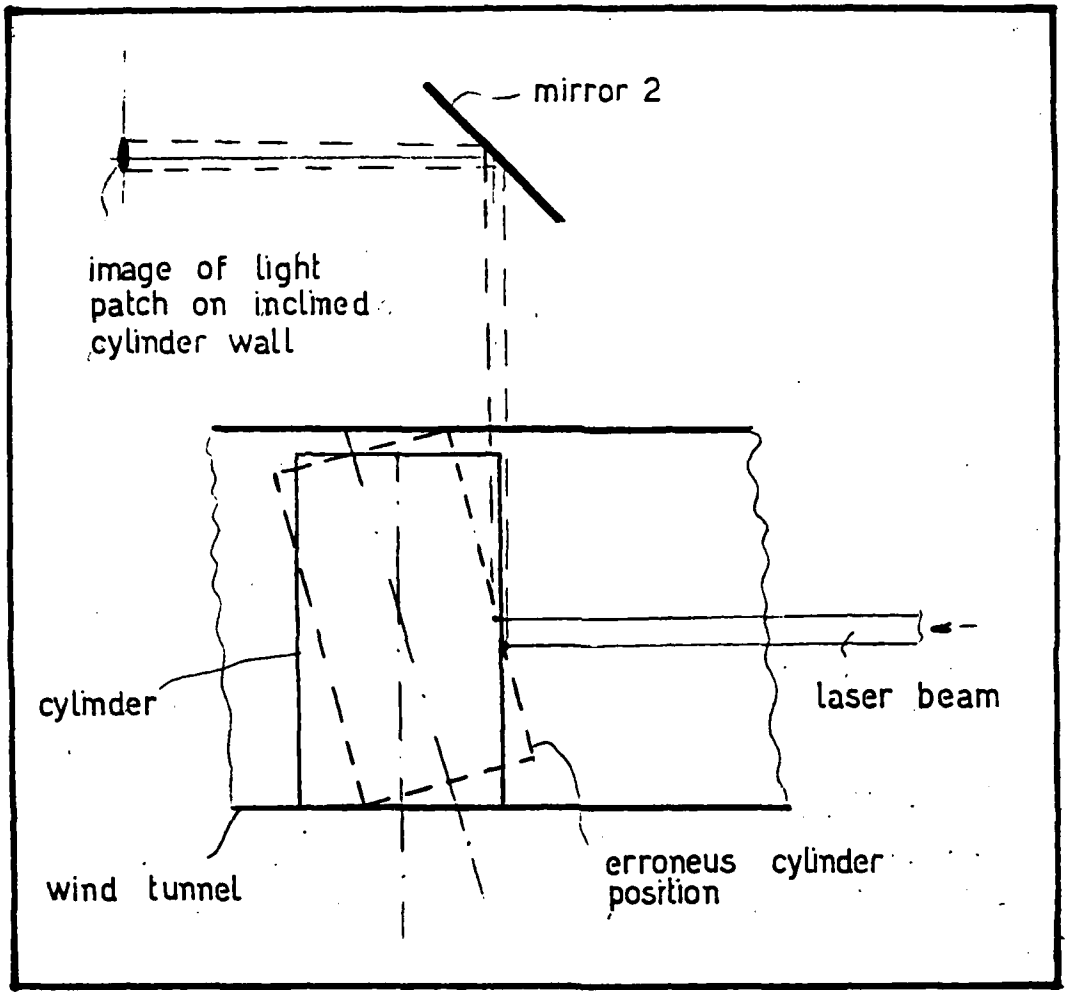

fig. 4.1.5: incorrect cylinder position as reflected in the collecting optics.

5. References

1. The use of coloured smoke to visualize secondary flows in a turbine-blade cascade, C.H. Sieverding, P. Van den Bosche; J. Fluid Mech., Vol. 134, 1983, pp. 85-89.

2. A visual study of turbin e blade pressure-side boundary layers, L.S. Han, W.R. Cox; J. Eng. for Power, January 1983, vol. 105, pp. 47-52.

3. Flow visualization in the tip region of a rotating blade row; W.R.C. Philips, M.R. Head; Int. J. Mech. Sci, Vol. 22, 1980, pp. 495-521.

4. Investigation of a tip clearance cascade in a water analogy rig; J.A.H. Graham, ASME Trans. J. of Eng. for Gas Turbines and Power, Vol. 108, Jan. 1986, pp. 38-46.

5. The automatic inspection of aerosol sprays using visual sensing; B.G. Batchelor; S.M. Cotter; Sensor Review, Jan. 1983, pp. 12-16.

6. Quantitative density visualization in a transonic compressor rotor; A.H. Epstein; ASME Trans. J. of Eng. for Power, July 1977, pp. 460-475.

7. Visualization of the flow at the tip of a high speed axial flow turbine rotor; J.P. Bindon, D. Adler; Report Technion - Israel Institute of Technology, June 1985.

8. A smoke generator for use in fluid flow visualization, Y.P.Yu, E.M. Sparrow, R.G. Eckert; Int. J. Heat Mass Transfer, Vol. 15, 1972, pp. 557-558.

9. Flow field measurement by tracer photography, R.J. Emrich, Experiments in Fluids, Vol. 1, 1983, pp. 179-184.

10. Applications of flow visualization techniques in aero-dynamics; C.M. Veret; SPIE Vol. 348, High Speed Photography (San Diego 1982), pp. 114-119.

11. Application d'un dispositif d'eclairage laminaire a la visualization des ecoulements aerodynamiques en souflerie par emission de fumee, M. Philbert; R. Beaupoil, J.P. Faleni; La Recherche Aerospatiale, no. 3, may - juin 1979, pp. 173-179.

12. Three-dimensional flow within a turbine cascade passsage; L.S. Langston, M.L. Nice; R.M. Hooper; J. of Engineering for Power, January 1977, pp. 21-28.

13. An experimental investigation of film cooling on a turbine rotor blade; R.P. Dring, M.F. Blair; H.D. Joslyn; J. of Engineering for Power, vol. 102, 1980, pp. 81-87.

14. Handbook of Physics, Condon & Odishaw, 1967, pp. 6-131-6-156.

15. Fluorescent minitufts for nonintrusive surface flow visualization; J.P. Crowder; IAA-A 82-20846; pp. 663 - 667.

16. The use of the dye-layer technique for unsteady flow visualization; M. Gad-el-Hak; Trans. ASME, J. of Fluids Engineering, Vol. 108, March 1986, pp. 34-38.

17. Laser -induced fluorescence visualization on supersonic mixing nozzles that employ gas-trips; A.A. Cenkner, R.J. Driscoll, AIAA Journal, vol. 20, no. 6, 1982, pp. 812-81 .

18. Velocity visualization in gas flows using laser-induced phosphorescence of biacetyl; B. Hiller, R.A. Booman, C. Hassa; R.K. Hanson; Rev. Sci. Instrum. 55(12), 1984, pp. 1964-1967.

19. Prospects for flow measurements based on spectroscopic methods, D. Baganoff.

20. Experimental comparison between laser Doppler anemometry and laser fluorescence anemometry; S. Beneech, F. Cignoli; A. Coghe, G. Zizak; Conf. Proc. Electro-Opt. Int' 80 U.K., pp. 233-240.

21. Laser-induced fluorescence technique for velocity field measurements in subsonic gas flows; B. Hiller, J.C. Mc Daniel, E.C. Rea, R.K. Hanson; Optics Letters, Vol. 8, no. 9, 1983, pp. 474-476.

22. The electric spark method for quantitative measurements in flowing gases - H.J. Bomelburg; J. Herzog, J.R. Weske, Z. Flugwiss, 7 (1959) Heft 11, pp. 322 - 329.

23. Expanded application programs of the spark tracer method with regard to centrifugal compressor impellers, W. Fister, J. Eikelman, U. Witzel; IAA Paper A82-20804, pp. 107-120.

24. Synthetic Dyes; E. Gurr; 1971; pp. 10-167.

25. Kodak-Laser Products Catalog - JJ-169; 1982; pp. 24.

26. Lasers; A.K. Levine, A.J. De Marila; Vol. 3, 1971.

27. Phorphorimetry in chemical analysis; W.J. McCarthy, J.D. Winefordner in: Fluorescence, G.G. Guilbault, 1967.

28. The Physical Chemistry of Dyeing; T. Vickerstaff; 1950; pp. 29-80.

29. Considerations sur le rendement de la fluorescence des solutions; I. Vierosanu; Rev. Roum. Phys., tome 11, no. 2, pp. 119-120, 1966.

30. Fluorescence and phorphorescence; P. Pringsheim; Interscience Publ. Inc. N.Y.; 1949, pp. 346-421.

31. Particle behaviour in flows and suitable particles for LDA measurements; A. Melling; Von Karman Inst. for Fluid Dynamics, Lecture series 1981-3.

32. A three-dimensional Laser-Doppler velocimeter for use in wind-tunnels; W.J. Yanta; ISCIAF-79 Record, pp. 294-301.

33. Tracer particle flow in a compressor rotor passage with applications to LDV; B.R. Maxwell; AIAA Journal, Vol. 13, no. 9, Sept. 1975, pp. 1141-1142.

34. Visualization by means of coherent light sheets: applications to different flows; R. Porcar, J.P. Prenel; Optics and Laser Technology; Oct. 1982, pp. 261-268.

35. Light scattering by small particles; H.C. van de Hulst; 1957, (pp. 14; 129; 264) ed. John Wiley & Sons Inc.

36. Fluorescence of aerosols; M. Kerker; Applied Optics, Vol. 12, no. 12, Dec. 1973; pp. 2787-2788.

37. Ealing Electro-Optics Inc. - data sheet for filter. 1986.

38. Image Intensifier - Philips data sheet 1987.

39. Measurement of drop sizes; B.J. Azzopardi; Int. J. Heat Mass Transfer, Vol. 22, 1979, pp. 1245-1299.

40. A study of a bluff-body combustor using laser-sheet lighting; W.M. Roquemore, R.S. Tankin; H.H. Chiu; S.A. Lottes, Experiments in Fluids, no. 4, 1986, pp. 205-214.

41. The generation and measurement of aerosols; A.G. Bailey; J. of Material Science 9, 1974, A.G. Bailey; J. of Material Science 9, 1974, pp. 1345-1363.

42. Fluid Mechanics, Frank M. White, 1979, McGraw-Hill, pp. 473-475.

43. Impingement of droplets in 90° elbows with potential flow; P.T. Hacker, R.J. Brun; B. Boyd; NACA TN 2999, Sept. 1953.

Appendix 1

COMPONENTS LIST

1. Wind tunnel
2. Cylinder ϕ 60
3. Bolt M6
4. Nut M6
5. Needle ϕ 0.5; ϕ 1
6. Disc A
7. Disc B
8. Needle support plate
9. Needle support pin M3
10. Screw M4
11. Nut M4
12. Retaining arm A.
13. Nut M6
14. Screw M6
15. Retaining arm B
16. Connecting hoose
17. Nut M3

section A-A
element 7 rotated by 90°
scale 1:1

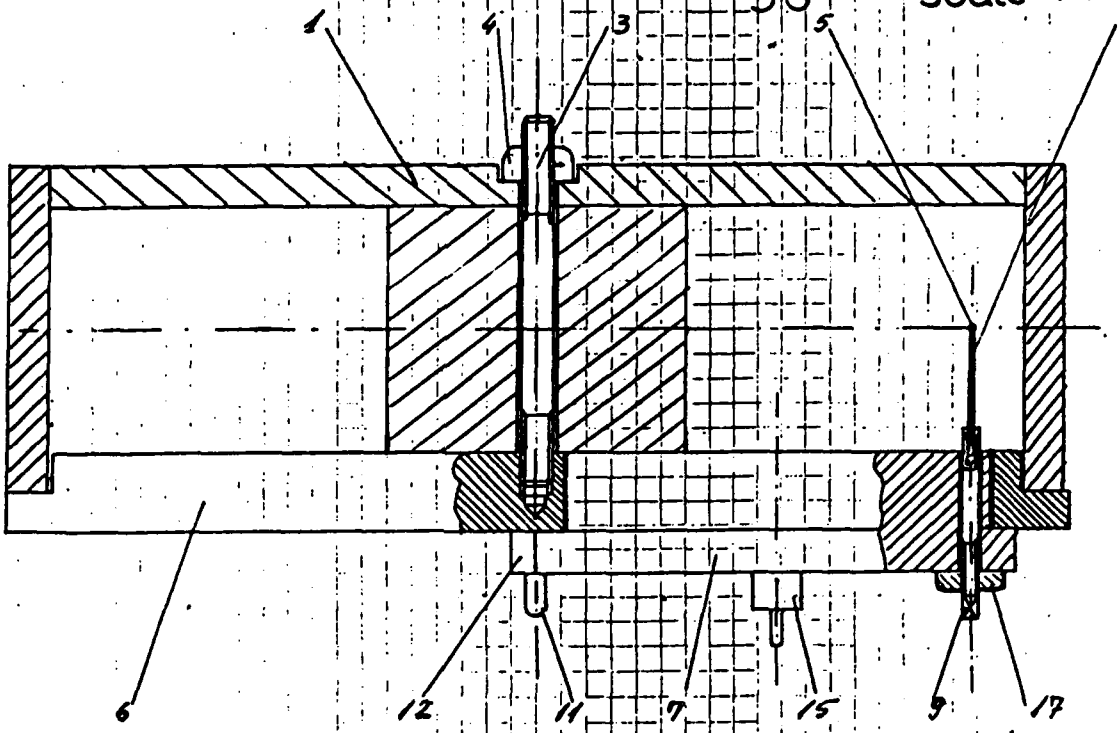

side view
scale 1:1

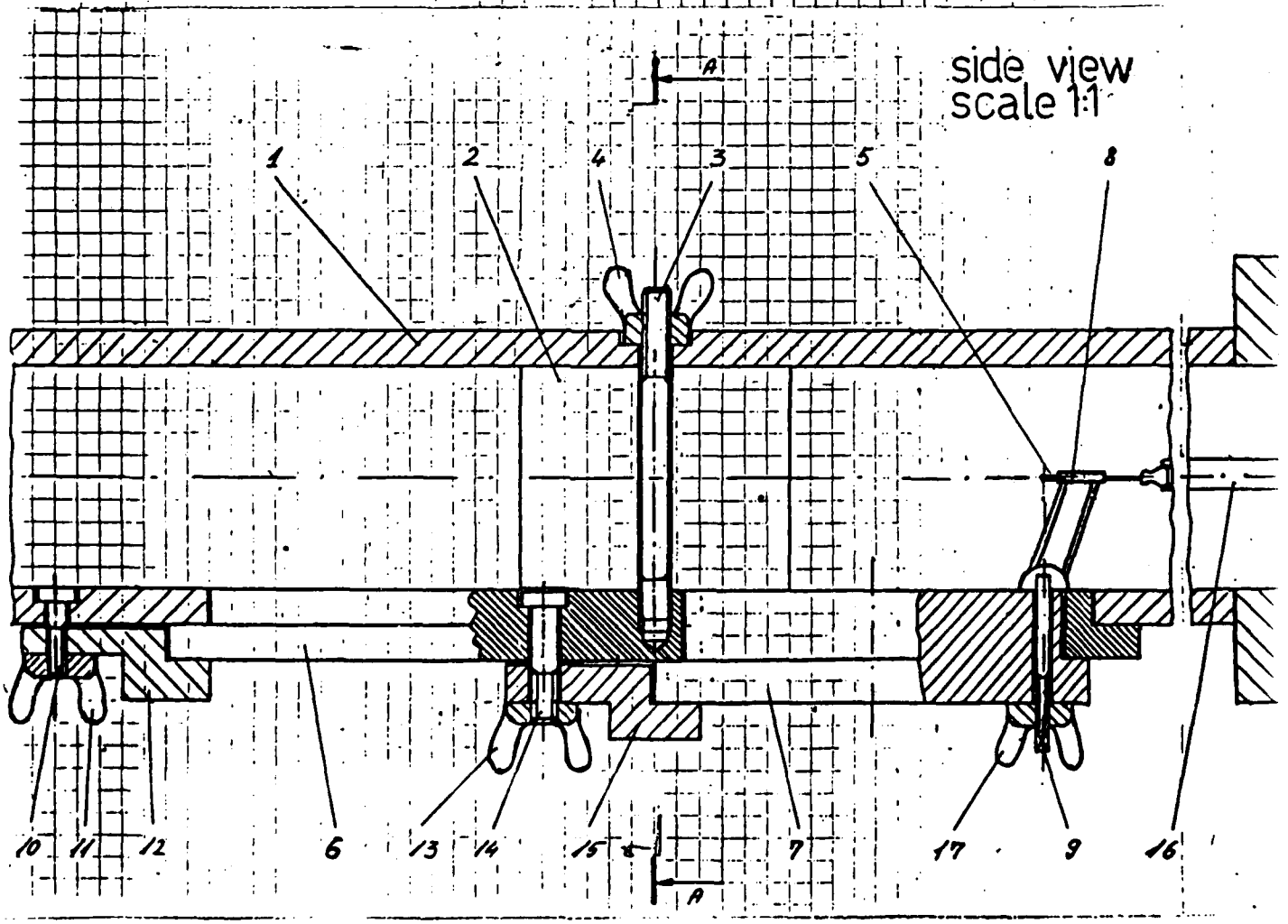

Appendix 2

Positioning of needle tip precision.

The precision analysis has been made in the following way:

Several starting points were chosen in the undisturbed inlet region of the flow (x_0 = -50mm, y_0 = 1.2 + 30 mm) fig. A.21. The streamlines corresponding to these points have tne general theoretical form (inviscid flow around a cylinder [42]:

For each point of these theoretical lines a pair of angles α and β (for the discs) has been calculated. If we assume that the marking on the discs allow for the distinction of 2.5^o; 2^o; 1^o or even fractions (0.2^o and 0.5^o) the calculated angles have to be rounded to the closest "readable" value; for example:

If $\alpha = 29.37^o$ (exact) then it has been rounded in the 2.5^o precision to $\alpha^* = 30.0^o$,

in the 1^o precision to $\alpha^{**} = 29.0^o$; in the 0.2^o precision to $\alpha^{***} = 29.4^o$.

For the "readable" set of angles the corresponding ψ/U_0 has been calculated. We set two limits for the $\Delta(\psi/u_0)$ between which we considered the "readable" point still associated with the same streamline ($\Delta_1 = \pm 0.16$ and $\Delta_2 = \pm 0.32$). see fig. A2-2. The points with "readable" angles falling outside these barriers were discarded. Only the first quarter was investigated at this stage. Fig. A2-3 and 4 summarize the results obtained from these calculations, for a starting point located at y_0 = 5mm.

It can be easily seen that the regions of higher curvature radiuses (2 and 3) are affected most significantly by the positioning precision: no "readable" point has been found to match the theoretical ones down to $+1^o$ in the 3 region. In the 2 region the number of points is also scarce. Only at 0.5^o or 0.2^o regions 2 and 3 can be mapped also. As one can expect if a larger $\Delta(\psi/U_0)$ is considered (± 0.32) the number of points in all the three regions is significantly increased.

As a first conclusion we stated that the positioning mechanism (discs) have to be improved up to fractions of degree (0.5 at least) in order to allow the mapping around the cylinder.

A more general conclusion is that for a complicated unknown flow, as around a blade, the positioning mechanis has to be automatised and its precision as high as possible.

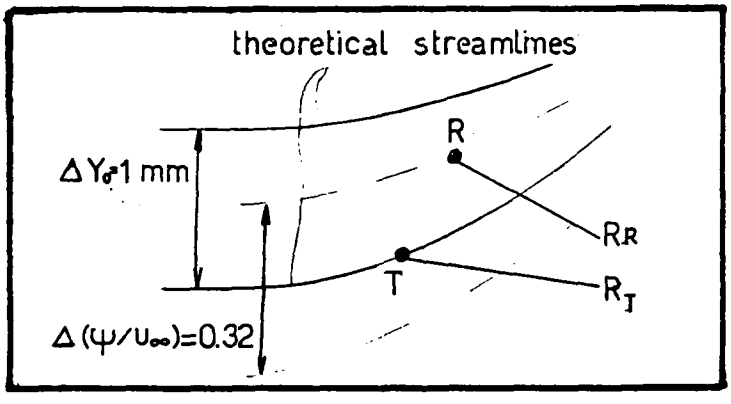

fig. A2-1: theoretical and real needle tip positioning.

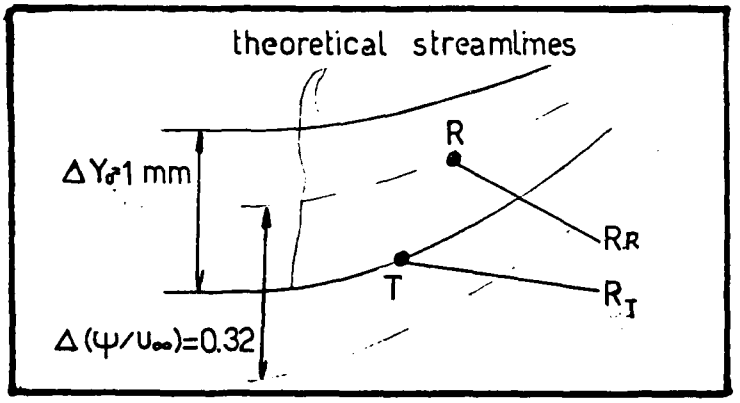

fig. A2-1: theoretical and real needle tip positioning.

Appendix 3

Droplet size evaluation.

We made an independent estimate using ref. [43]. For a potential flow in a 90^{o} elbow the following collection efficiencies were calculated:

12% for 10μm diameter droplets and

57% for 25μm diameter droplets.

For a 180^{o} turn as in our case we obtain that 77.5% of the 10 μm diameter droplets passed through the elbow but only 26.8% of the 25μm diameter ones. Although the conditions for the calculation of the collection coefficients are different in ref. [43] than ours (both geometrical and thermodynamical) we concluded that our conditions do favorize higher separation rates (collection coefficients) because higher temperatures, lower velocites, vertical flow a.s.o.

Our atomizing apparatus is of the "aerodynamic dispersion" type [41]. The atomizer (fig. 3.2.3-1) has the role of creating a primary dispersion in the air jet of the liquid. According to [41] "the baffles intercept the greater portion of the aerosol flow from the atomizer head...". In the case of a very similar apparatus (the "Collison nebulizer" [41]) with one 180^{o} turn in the air flow, operating at air-pressure in the range 15 to 50 psi (same as ours), reference [41] states that: "...The baffles intercept the majority of droplets having diameters greater than about 10μm although a few large droplets .... are emitted." "With water a few drops of 55 μm are detectable". ".... as much as 99.92% of the atomized liquid is refluxed back into the reservoir".

Finaly we can estimate that most droplets were under 10μm diameter.

Appendix 4

Alignment procedure: step 1:

Establishing the parallelism between the laser beam and the wind tunnel.

a) The mirror placed on the laser beam path (at any angle φ) deviates the beam to the mirror b) placed on the external wall of the wind tunnel. The point 1" is seen with the aid of a target and the distance δ_1 recorded. A second position (2") is then obtained by moving the mirrors forward. If the distance δ_2 is smaller than δ_1 then the deviation angle α is positive (see figure) and the correction has to be made in the opposite direction, until δ_2 becomes equal to δ_1.

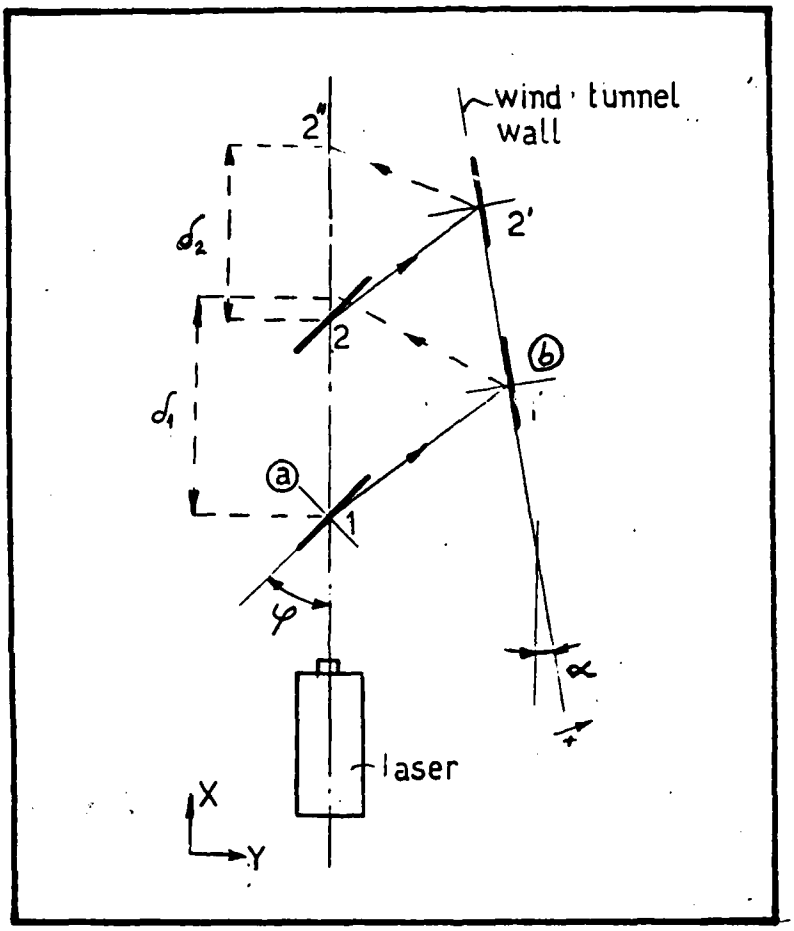

fig A4-1: alignement procedure for parallelism of laser beam to wind tunnel wall.

Alignment procedure: step 2:

Establishing the perpendicularity of the laser beam to the wind tunnel axis.

The mirror ⓐ placed on the laser beam path at an angle φ_1 (any) deviates the beam to the mirror ⓑ placed on the external wall of the wind tunnel. If the angle φ_1 is not 45^o then point 1" falls behind the mirror ⓐ. By rotating the mirror ⓐ the correct position can be obtained ($\delta_2 = 0$).

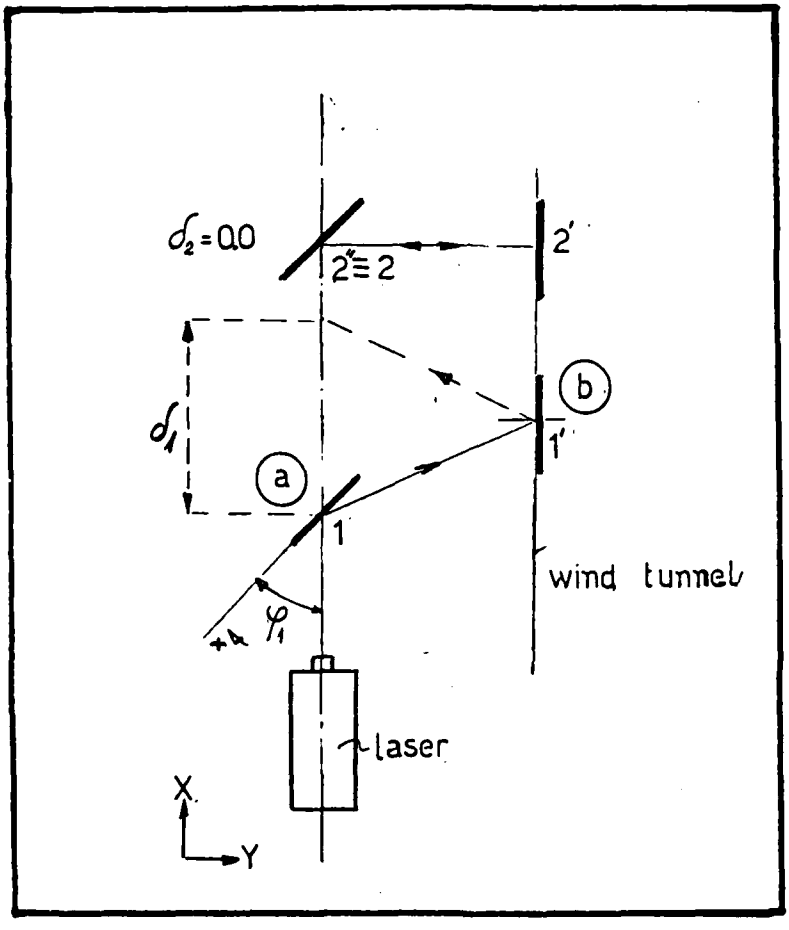

fig. A4-2: alignement procedure for perpendicularity of laser beam to wind tunnel wall.

Alignment procedure: step 3:

Establishing the perpendicularity of the reflected beam to the wind tunnel axis.

A target has been mounted in the place of the image intensifier (at the height H-calculated). The mirror b placed in the wind tunnel reflects the incident laser beam at 45^{o} upwards. By adjusting the position of the mirror ⓒ - mounted on the wind tunnel - the reflected beam is directed to the target such as δ_1 and δ_2 become zero. The operation is repeated for several positions along the wind tunnel.

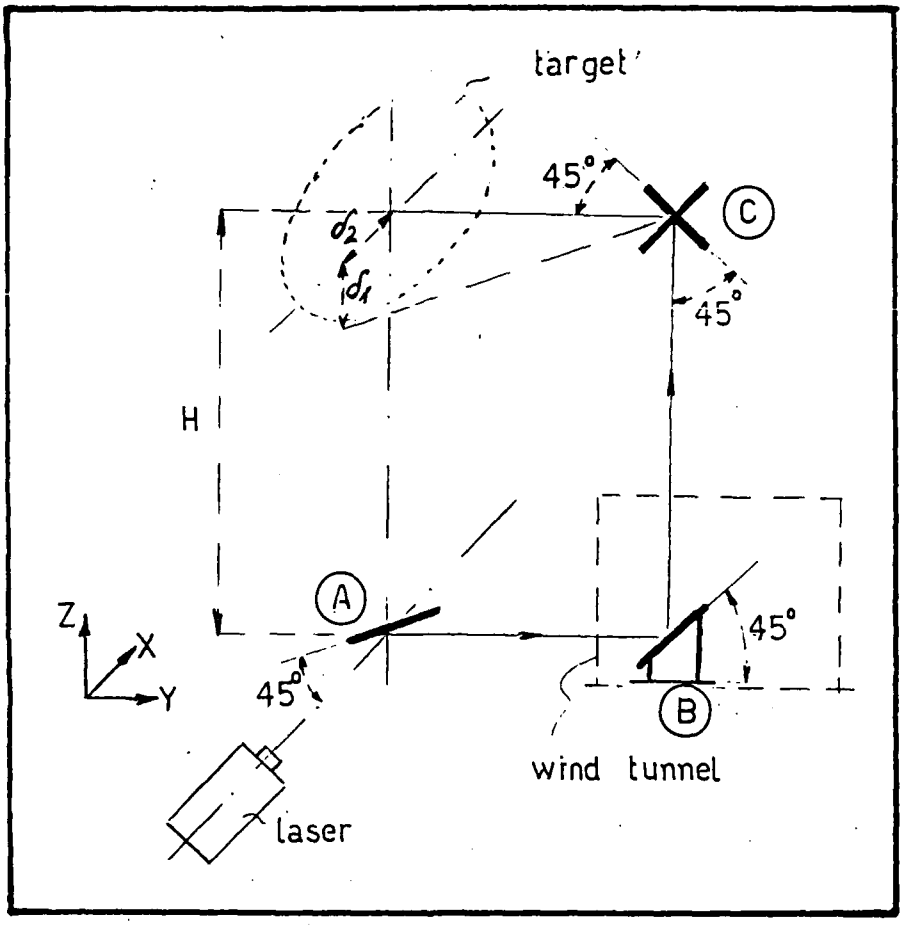

fig. A4-3 : alignement procedure for the perpendicularity of the collecting optics axis to the wind tunnel axis.


DAT
FILM